

# JGR Space Physics



## RESEARCH ARTICLE

10.1029/2023JA031861

### Key Points:

- An aurorally aligned subcorotational thermospheric vortex is detected in Jupiter's upper atmosphere
- Two sunward ionospheric jets flowing through the thermosphere are revealed on both dawn and dusk
- Jupiter potentially has a multilayer ionosphere driven separately by asymmetric currents and breakdown-in-corotation Pedersen currents

### Supporting Information:

Supporting Information may be found in the online version of this article.

### Correspondence to:















R. Wang,  
[rw318@leicester.ac.uk](mailto:rw318@leicester.ac.uk)

### Citation:

Wang, R., Stallard, T. S., Melin, H., Baines, K. H., Achilleos, N., Rymer, A. M., et al. (2023). Asymmetric ionospheric jets in Jupiter's aurora. *Journal of Geophysical Research: Space Physics*, 128, e2023JA031861. <https://doi.org/10.1029/2023JA031861>

Received 7 JUL 2023  
Accepted 14 NOV 2023

## Asymmetric Ionospheric Jets in Jupiter's Aurora

Ruoyan Wang<sup>1</sup> , Tom S. Stallard<sup>2</sup> , Henrik Melin<sup>1</sup> , Kevin H. Baines<sup>3,4</sup> , Nicholas Achilleos<sup>5</sup> , Abigail M. Rymer<sup>6</sup> , Licia C. Ray<sup>7</sup> , Jonathan D. Nichols<sup>1</sup> , Luke Moore<sup>8</sup> , James O'Donoghue<sup>9</sup> , Mohammad N. Chowdhury<sup>1</sup> , Emma M. Thomas<sup>1</sup> , Katie L. Knowles<sup>2</sup> , Paola I. Tiranti<sup>1</sup> , and Steve Miller<sup>5</sup>

<sup>1</sup>School of Physics and Astronomy, University of Leicester, Leicester, UK, <sup>2</sup>Department of Mathematics, Physics and Electrical Engineering, Northumbria University, Newcastle upon Tyne, UK, <sup>3</sup>Jet Propulsion Laboratory, California Institute of Technology, Pasadena, CA, USA, <sup>4</sup>Space Science and Engineering Center, University of Wisconsin-Madison, Madison, WI, USA, <sup>5</sup>Department of Physics and Astronomy, University College London, London, UK, <sup>6</sup>Applied Physics Laboratory, Johns Hopkins University, Laurel, MD, USA, <sup>7</sup>Department of Physics, Lancaster University, Lancaster, UK, <sup>8</sup>Center for Space Physics, Boston University, Boston, MA, USA, <sup>9</sup>Institute for Space and Astronautical Science, JAXA, Sagami, Japan

**Abstract** Simultaneous infrared observations of H<sub>3</sub><sup>+</sup> and H<sub>2</sub> emissions from Jupiter's northern aurora using the Near Infrared Spectrograph at Keck Observatory were used to measure the ionospheric and thermospheric wind velocities. H<sub>3</sub><sup>+</sup> ions supercorotate near the dawn auroral oval and subcorotate across the dusk sector and in the dawn polar region relative to the planetary rotation rate, broadly in agreement with past observations and models. An anticyclonic vortex is discovered in H<sub>2</sub> flows, closely matching the mean magnetospheric subcorotation when the observed magnetospheric flows are averaged azimuthally. In comparing ion and neutral winds, we measure the line-of-sight effective ion drift in the neutral reference frame for the first time, revealing two blue-shifted sunward flows of ~2 km/s. Observed H<sub>3</sub><sup>+</sup> and H<sub>2</sub> emissions overlap with predictions of the Pedersen conductivity layer, suggesting two different regions of the ionosphere: (a) a deep layer, where neutral forces dominate the thermosphere and symmetric breakdown-in-corotation currents can close, and (b) a higher layer, where the observed effective ion drift allows dawn-to-dusk Pedersen currents within the upper atmosphere, in turn closing asymmetric currents within the magnetosphere. This ionospheric structure aligns well with recent Juno observations of Jupiter's aurora. The detected thermospheric vortex implies the driving of neutral flows by the momentum from the magnetosphere within the thermosphere and deeper in the atmosphere to potentially 20 mbar. Jovian neutral thermosphere might bridge the gap between current observations and modelings and perhaps be significant to the dynamics of aurora on Earth and other outer planets.

**Plain Language Summary** We observed both charged and neutral molecules in Jupiter's northern aurora from the Keck Observatory. The velocity of the charged particles shows that they are controlled by magnetic field lines that stretch into the surrounding space environment, as expected at the top of the atmosphere. However, neutrals at the top of the atmosphere also appear to be indirectly controlled by the magnetic field, driven by impacts with the ions into a large vortex that sits within Jupiter's auroral region. Because the charged and neutral molecules move differently from one another, this can drive high-altitude currents. Charged particles flow through the neutrals in two jets, moving toward the Sun on both sides of Jupiter's aurora, driving asymmetric currents more like the system of currents that form Earth's aurora. It suggests that Jupiter has different currents closing at different altitudes in the auroral region. This layering of currents matches recent observations made by the Juno mission and may help explain some of the apparent conflicts between different Juno data sets. Our discovery also highlights the importance of interactions between charged and neutral particles on other planets, including Earth, making Jupiter an important comparator for future studies of these interactions.

## 1. Introduction

The dominant theory regarding the generation of Jupiter's aurora in the past few decades has been linked to the motion of magnetospheric plasma surrounding the planet, widely known as the breakdown-in-corotation theory (Hill, 1979). Ionospheric plasma that is collisionally coupled to the neutral atmosphere is linked along magnetic field lines to plasma in the magnetospheric equatorial plane, at distances where the Keplerian orbit forces the plasma to significantly subcorotate. Close to the planet, the magnetospheric plasma instead moves with the underlying neutral atmosphere, because of the strength of the viscous torque exerted by ion-neutral collisions in the

© 2023. The Authors.

This is an open access article under the terms of the [Creative Commons Attribution-NonCommercial-NoDerivs License](https://creativecommons.org/licenses/by-nc-nd/4.0/), which permits use and distribution in any medium, provided the original work is properly cited, the use is non-commercial and no modifications or adaptations are made.

planetary atmosphere. This torque is transmitted to the magnetosphere by field-aligned currents, which converge to flow radially outward through the plasma disc, providing a  $\vec{j} \times \vec{B}$  force that acts to maintain corotation with the planet. As the plasma moves radially outward, the energy required to maintain corotation increases, so that eventually it cannot be sustained by a torque from the neutral atmosphere. This results in a breakdown in corotation, where the magnetospheric plasma slows azimuthally. Field-aligned currents continue to feed radial currents through this subcorotating region, closing via Pedersen currents in the ionosphere. Early models suggest that the main auroral emission is generated by particle accelerations associated with upward field-aligned currents driving electrons into the atmosphere (Cowley & Bunce, 2001; Hill, 1979, 2001), though more recent work indicates that the main auroral emissions are linked to both upward and downward currents (Mauk et al., 2020).

Pedersen currents that close breakdown-in-corotation currents occur at altitudes where ionospheric flows transition from the domination of the magnetosphere to the atmosphere, thereby modulating their effectiveness to enable magnetospheric currents to close through planets. Due to the difficulty of modeling ionosphere-magnetosphere interactions in Jupiter, all models have been forced to make assumptions that limit our understanding of the extent and effect of the coupling between the atmosphere and the magnetosphere. Yates et al. (2020) modeled Jupiter's upper atmosphere by coupling a 3-D atmospheric general circulation model to an axisymmetric magnetosphere. Constructed on the basis of various models from previous studies, the model built a solid foundation for simulating self-consistently coupled 3-D atmosphere-magnetosphere systems. This intermediate step suggests the possibility of using predictions from various models to attempt to predict the broad-scale ion and neutral coupling within Jupiter's atmosphere.

As of yet, however, models including the effects of asymmetric magnetospheric flows within a 3-D neutral thermosphere have not been explored in depth, leaving a gap in understanding how the atmospheres of fast-rotating planets couple with the surrounding magnetosphere. Asymmetric features within the jovian aurora have been reported in several recent studies, highlighting a growing body of evidence that appears contradictory to an axisymmetric system (Bonfond et al., 2020), the main assumption of models based on the breakdown-in-corotation theory (Cowley & Bunce, 2001). The lack of complex modeling may help explain recent controversies in the observed aurora of Jupiter.

### 1.1. Pedersen Conductivity, Effective Pedersen Conductivity, and Neutral Wind Driven Current Systems

Because no models of ionosphere-magnetosphere coupling up to date include longitudinal variations in both the atmosphere and magnetosphere, the driving mechanism of currents within the atmosphere by asymmetric flows in the magnetosphere or the impact onto these currents by ion-neutral coupling is not fully understood. However, numerical simulations (e.g., Yates et al., 2020, and references therein) provide complementary information about how these interactions will occur, so we can use their outcomes to speculate about the likely interactions between an asymmetric magnetosphere and the underlying atmosphere.

Figure 1a presents a cartoon of varying ion and neutral velocities with altitude, based upon the original presentation of these values from Hill (1979), adapted to better match the changing ion and neutral velocities using a simplification of flows modeled in Tao et al. (2009). It highlights the location of the  $\vec{E} \times \vec{B}$  motion, which in turn drives a meridional Pedersen current that closes the field-aligned currents flowing into and out of the magnetosphere, here representing a rotational symmetric atmosphere.

The classic definition of the upper extent of the Pedersen conductive layer is the boundary at which the ion-neutral collision frequency falls below the ion gyrofrequency. Figure 1b shows how the ratio of gyrofrequency ( $\omega_c$ ) over ion-neutral collision rate ( $\nu_{ni}$ ) changes with altitude (light and dark, solid and dashed lines). The ratio is dominated by the exponential decrease in  $H_2$  density and is exacerbated by the decreasing magnetic field with altitude, so that the wide range of Jupiter's surface field strength results in a relatively small altitudinal range for the top of the Pedersen conductivity layer. In this altitudinal region, ions interact with the neutral atmosphere, whereas electrons do not.  $\vec{E} \times \vec{B}$  drift, the product of the electric field imposed by field-aligned currents, causes ions to move perpendicular to the electric field, but impacts with the surrounding neutral atmosphere force these ions to drift in the direction of the imposed electric field, while electrons continue to flow unimpeded. This results in a perpendicular Pedersen current that closes field-aligned auroral currents. However, when there are many impacts within a molecule gyrorotation ( $\omega_c/\nu_{ni} < \sim 0.01$ ), the ions become entrained in the surrounding neutral atmosphere, prevented from undergoing strong  $\vec{E} \times \vec{B}$  drift, producing significant Hall currents but limited Pedersen currents.

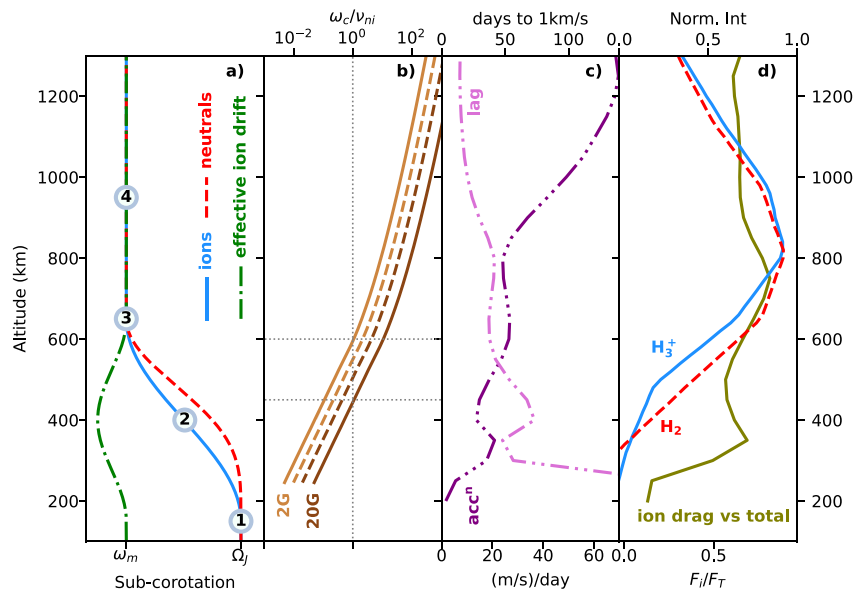


**Figure 1.** Jupiter's ionosphere/atmosphere coupling with altitude. In the left column, panel (a) shows a simplified illustration of the changing ion (solid blue) and neutral (dashed red) winds with altitude, as a value of subcorotation ranging between  $\Omega_J$  (full rotation with the underlying atmosphere) and  $\omega_m$  (full subcorotation in alignment with the magnetosphere when mapped along magnetic field lines). At low altitudes ①, both the ionosphere and atmosphere are dominated by neutral atmospheric forces, corotating with the planetary interior  $\Omega_J$ . As the collision rate drops with increasing altitude ②, ions increasingly subcorotate ( $\Omega_J \rightarrow \omega_m$ ) until they move with the subcorotation of the magnetically mapping equatorial magnetosphere  $\omega_m$  ③. As ion drag becomes the dominant accelerating force in the atmosphere (highlighted in panel (c)), neutrals are also accelerated away from corotation ②. Where the ion drag dominates completely ③, neutrals also subcorotate with the magnetosphere, reducing the effective Pedersen conductivity to zero. Above this, the true Pedersen conductivity also drops to zero ④. Panel (b) shows the changing  $\omega_c/\nu_{ni}$  ratio with altitude, calculated for surface field strengths of 2, 4, 8, and 20 G (solid light brown, dashed light brown, dashed dark brown, and solid dark brown lines, respectively), representative of magnetic field strengths within Jupiter's main auroral emission region. The upper boundary of the Pedersen conductive layer is approximately located where  $\omega_c/\nu_{ni} < 1$  (with this value indicated by a vertical dotted line, and the altitude where this occurs for surface field strengths of 2 and 20 G indicated by horizontal dotted lines). Panel (c) shows the expected neutral acceleration caused by ion drag over a jovian rotation (three-dot dashed purple line), calculated from Tao et al. (2009), and the related lag in accelerating the atmosphere by 1 km/s in jovian days (noted in the axis as “days to 1 km/s”; two-dot dashed pink line). Panel (d) shows the normalized altitudinal  $H_3^+$  and  $H_2$  emission presented in Kita et al. (2018) (solid blue and dashed red line, respectively), from emission lines used in this study. It also shows the fractional strength of the ion drag acceleration force  $F_i$  when compared against all acceleration forces affecting the neutral atmosphere  $F_T$  (solid olive line).

The ion flows shown in Figure 1a reflect the extent of  $\vec{E} \times \vec{B}$  drift allowed. At the base of the atmosphere ①, both the neutral atmosphere (dashed red) and the co-located ionosphere (solid blue) are coupled with the underlying interior and so move with the rotational period of Jupiter's interior  $\Omega_J$ . At higher altitudes ②, starting around 200–300 km (Tao et al., 2009), the reduced collision rate allows the influence of the magnetosphere to grow, forcing the ions to be accelerated by  $\vec{E} \times \vec{B}$  forces to some extent of subcorotation. This  $\vec{E} \times \vec{B}$  driven subcorotation strengthens with altitude until the ionosphere moves with the velocity of the magnetosphere  $\omega_m$ , when mapped along magnetic field lines from the magnetospheric equator to the planet. From this altitude ③ upward, the ions remain in subcorotation with the magnetosphere. Notably, since the aurora is neither circular nor aligned with the jovigraphic rotational pole, this “subcorotation” does not manifest simply as a reduction in the planetary rotation rate, but instead as an ionospheric vortex that has the same velocity as magnetic field lines close to the planet's surface. At even higher altitudes ④, the Pedersen conductivity  $\Sigma_p$  falls away, so no matter what  $\vec{E} \times \vec{B}$  drift occurs, Pedersen currents cannot be carried through the atmosphere. Note that the atmosphere is still collisionally linked to the ions at this altitude, in local thermal equilibrium until >1,000 km (Tao et al., 2011) and to the ion drag peaking at ~1,500 km (Tao et al., 2009).

Field-aligned currents originating from the magnetosphere must close through Pedersen currents within the ionosphere. Hence, as at Earth, the ionosphere is only able to close currents from the magnetosphere in layers with strong Pedersen conductivity. On Earth, calculations of Pedersen currents generated by  $\vec{E} \times \vec{B}$  drift typically

assume that the neutrals are stationary. However, if the neutral atmosphere is moving in the direction of the ion drift, the momentum transferred from the neutrals will mitigate this upward drift, as the Pedersen currents produced by  $\bar{\mathbf{E}} \times \bar{\mathbf{B}}$  drift are properly considered in the rest frame of the surrounding neutral atmosphere. As ions drift through the neutral atmosphere, the same collisions that drive the Pedersen currents also accelerate the neutral atmosphere in the direction of this  $\bar{\mathbf{E}} \times \bar{\mathbf{B}}$  drift. As the neutrals start to move with the ions, the  $\bar{\mathbf{E}} \times \bar{\mathbf{B}}$  drift slows in the rest frame of the neutrals, preventing the ions from moving in the direction of the imposed electric field and attenuating the resultant Pedersen current.

At Jupiter, because the magnetosphere drives the  $\bar{\mathbf{E}} \times \bar{\mathbf{B}}$  drift to subcorotate around the entire main auroral emission, these flows are symmetric around the magnetic pole of the planet. Ion drift flows in the same symmetric direction regardless of the rotational phase of the planet. This allows the ion drag to slowly build neutral flows with time, so that the steady-state neutral atmosphere moves at a fractional amount of the ions, a coupling term known as  $k$  (where  $k = 0$  has the neutrals corotating with the interior of the planet, and  $k = 1$  has them moving with the ionosphere; Huang & Hill, 1989). In the past, the reduction of Pedersen currents through the acceleration of neutrals has been modeled by scaling the true Pedersen conductivity  $\Sigma_p$  by the relative velocities between ions and neutrals in the rest frame of the planet (Huang & Hill, 1989). This reduced “effective Pedersen conductivity”  $\Sigma_p^*$  accounts for neutral winds reducing the Pedersen currents available for field-aligned currents closing in the magnetosphere, which in turn decrease the predicted auroral brightness (Cowley et al., 2003).

Here, rather than calculating an effective Pedersen conductivity, we instead examine the Pedersen current generation by considering the  $\bar{\mathbf{E}} \times \bar{\mathbf{B}}$  ion drift only with respect to the reference frame of the surrounding neutral atmosphere: taking the difference between the ion and neutral flows, defined here as the “effective ion drift.” The advantage of considering the effective ion drift is that both ion and neutral wind velocities can be observed from Earth, allowing the line-of-sight effective ion drift to be measured directly, providing observable estimates of the direction and strength of the resultant Pedersen currents driven by this drift.

The extent to which the neutral atmosphere is forced into motion with the ionosphere changes with altitude. With increasing altitude, the ion drag exerted on molecules within the neutral atmosphere also increases, as described in Tao et al. (2009) and shown as a three-dot dashed purple line in Figure 1c. However, ions and neutrals also continue to feel other accelerating forces (Coriolis, viscosity, and meridional advection), so the extent to which ions and neutrals can move into subcorotation with the magnetosphere is strongly influenced by the changing dominance of ion drag as an accelerating term in the atmosphere. Figure 1d (solid olive line) shows the fractional strength of the ion drag acceleration force  $F_i$  compared to all acceleration forces that affect the neutral atmosphere  $F_T$ . This altitude dependence, calculated using various horizontal acceleration terms shown in Tao et al. (2009), highlights how ion drag is a very weak term at low altitudes ①, becoming quickly dominant in the main ionospheric region ②, and even more dominant in the region where the ionosphere and neutral atmosphere match in subcorotation ③. Above  $\sim 1,500$  km, the dominance of ion drag quickly disappears again as the Coriolis and viscosity forces are significantly strengthened.

The effects of this coupling can be seen in Figure 1a. At low altitudes ①, even though there is significant true Pedersen conductivity  $\Sigma_p$ , ions and neutrals are completely coupled by collisions, the effective ion drift is stationary in the neutral frame, the effective Pedersen conductivity  $\Sigma_p^*$  is zero and there are no Pedersen currents.

At moderate altitudes ②, the ion drag is partially balanced by other forces in the atmosphere, so the ions cannot move at the full subcorotation of the magnetosphere  $\omega_m$ , and the steady-state neutral atmosphere moves at a fraction of the ions, so that the coupling term ( $k$ , Huang & Hill, 1989), ranges between  $0 > k > 1$ . Since ions move relative to the reference frame of the surrounding neutral atmosphere, the effective ion drift (dashed green line) can produce a Pedersen current in this region, with the effective Pedersen conductivity ( $\Sigma_p^*$ ) a function of the relative velocity of ions and neutrals ( $k$ ) and the true Pedersen conductivity ( $\Sigma_p$ ).

At higher altitudes ③, the neutral atmosphere is accelerated by ion drag into full subcorotation  $\omega_m$ , so the neutral atmosphere moves with both the ionosphere and the magnetosphere ( $k = 1$ ). Despite the significant  $\bar{\mathbf{E}} \times \bar{\mathbf{B}}$  drift, the effective ion drift velocity is zero; this  $\bar{\mathbf{E}} \times \bar{\mathbf{B}}$  drift is unable to drive a Pedersen current and therefore the effective Pedersen conductivity  $\Sigma_p^*$  is again zero. (Here, for clarity of argument, we assume that this layer has significant True Pedersen conductivity—in reality, the uppermost conducting layers are only extremely limited by the motion of neutrals (with  $k > 0.8$ ), instead of completely nullified.)

The upper ionosphere ④ sits well above the upper limit for True Pedersen Conductivity, so the relative motions of ions and neutrals are no longer important. Tao et al. (2009) highlight how the ions and neutrals decouple in this region, as their calculated  $k$  factor rises above 1, as high as 10 at the top of the atmosphere, as other terms force

the neutrals into even more westward flows, significantly subcorotating in the perspective of the magnetosphere (velocities  $< \omega_m$ ), and yet generating no currents.

However, even where the ion drag is the dominant accelerating force in the atmosphere, this acceleration is still very slow. As shown in Figure 1c, Tao et al. (2009) predict significant lag between ions and neutrals (two-dot dashed pink line), with a 1 km/s ion wind taking  $\sim 40$ –60 jovian days to force the neutral atmosphere to match its motion in the main ionospheric region (300–600 km) and hundreds of days at the base of the ionosphere ( $< 250$  km). As a result, while models that estimate the coupling between ions and neutrals provide a good approximation of the effective Pedersen conductivity in a steady state and axisymmetric system, where the  $\vec{E} \times \vec{B}$  drift produced by magnetospheric currents is changing “quickly” (on a timescale of  $< 40$  rotations), these models will significantly overestimate  $k$ , as neutrals will not move with the ionosphere. As a result, temporal (e.g., due to changing solar wind conditions, reconfigurations in the magnetotail or volcanic output of Io) or spatial (e.g., due to asymmetric magnetospheric velocities, or dynamic solar wind pressure that distorts the magnetic field mapping) variability in the  $\vec{E} \times \vec{B}$  drift will allow significant currents to flow, even in altitudinal regions where models predict that neutrals will match with ions ( $k = 1$ ) and have no effective Pedersen conductivity ( $\Sigma_p^* = 0$ ).

The most notable example of variable  $\vec{E} \times \vec{B}$  drift comes from the asymmetric ion velocities observed between dawn and dusk in both magnetospheric and ionospheric flows (e.g., Johnson et al., 2017; Krupp et al., 2001; Stallard et al., 2001). For such flows, the ions will move asymmetrically between dawn and dusk far faster than the surrounding neutral atmosphere. An understanding of how these asymmetric flows affect Pedersen currents within the ionosphere can be provided by the effective ion drift within the ionosphere. To do this, we must simultaneously measure both ion and neutral wind velocities within the same layer of the atmosphere. Fortunately, measurements of emission from the quadrupole  $H_2$  and overtone  $H_3^+$  lines at high spatial resolution have shown that these species emit from the same altitudinal range of  $\sim 700$ –900 km (Kita et al., 2018; Uno et al., 2014). This very close alignment in emission altitudes, shown in Figure 1d, places them just above the Pedersen conductive layer, in the region ④ of Figure 1a.

Although only a fraction of  $H_2$  and  $H_3^+$  emission originates within the true Pedersen conductivity layer (and is therefore capable of carrying Pedersen currents), both  $H_2$  and  $H_3^+$  sit comfortably within the region dominated by the ion drag, with this drag changing very slowly over time, as shown in Figures 1c and 1d. As a result, the corresponding flows in the underlying Pedersen conductive atmosphere (layers ② and ③) will closely resemble the flows observed in the upper atmosphere, changing only as a result of the varying coupling between the ions and neutrals. In the next section, we assess the likely ion and neutral winds and how this atmospheric coupling produces a varying effective ion drift with altitude, resulting in a changing Pedersen current.

## 1.2. Asymmetric Magnetospheric Effects on Ionospheric and Neutral Flows

Figure 2 provides a cartoon of the observable ionospheric flows and auroral emissions for both axisymmetric and asymmetric models, along with the estimated neutral winds and the resultant effective ion drift. In the left column of Figure 2, we show the axisymmetric case, based upon the Cowley et al. (2003) model. At the top of the column is a cartoon representation of the ion winds and auroral emissions viewed from above. The breakdown in corotation within the magnetosphere results in increasingly westward flows toward the pole of the planet ( $S_V$ ), driving an axisymmetric auroral emission ( $S_E$ ). Below this, we provide a representation of the resultant ion and neutral flows, which might be observed from Earth using line-of-sight Doppler shifts, at the three representative altitudes ①, ②, and ③ shown in Figure 1a. At the bottom of the atmosphere (S1), ions (solid blue line), and neutrals (dashed red line) corotate with the planet, producing a positive blueshift at dawn and a negative redshift at dusk. However, because they match in velocity, the ions are stationary in the neutral reference frame, resulting in no effective ion drift (dotted dashed green line). Above this, in the peak Pedersen conductivity layer (S2), polar ions linked to the outer magnetosphere significantly subcorotate (Cowley et al., 2007), while equatorward of the auroral region, ions rotate with the planet, with a gradient in ion winds between these extremes. Neutrals subcorotate more gently (here  $k = 0.5$ ), resulting in a measurable subcorotational difference in these velocities and thus a line-of-sight measurement of the effective ion drift that matches with the true ion drift (scaled by  $1 - k$ , here 0.5), observed as the line-of-sight component of this drift. This effective ion drift allows an effective Pedersen conductivity to exist, so that a (weakened) Pedersen current closes the field-aligned breakdown-in-corotation currents through the atmosphere. At higher altitudes (S3), both ions and neutrals strongly subcorotate together under the force of the magnetospheric torque. Consequently, there is no effective ion drift and therefore no Pedersen currents are

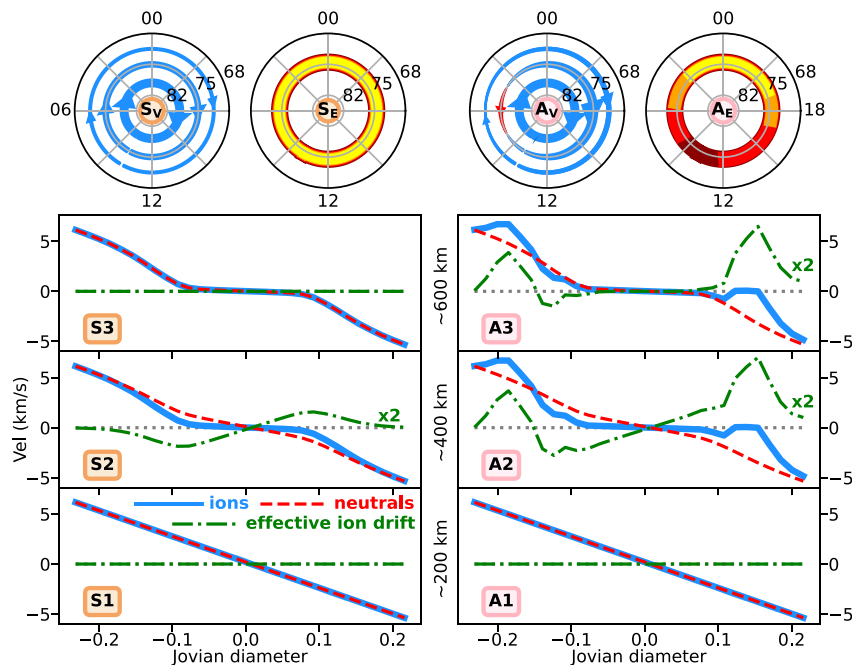


**Figure 2.** A cartoon representation of ion and neutral winds in Jupiter's atmosphere. In the left column, we show the velocity structures associated with the Cowley et al. (2003) axisymmetric model. In the right column, we show our prediction of the velocity structures produced by the Chané et al. (2013) asymmetric model. At the top of both columns, a polar view of the planet is shown, with latitude plotted radially and local time plotted, highlighting the ion wind velocity structures predicted for the ionosphere ( $S_V$  and  $A_V$  for Cowley et al. (2003) and Chané et al. (2013), respectively), with velocities in the planetary frame (blue for subcorotation and red for supercorotation). Also shown at the top is a simplified representation of the auroral emission predicted by each model ( $S_E$  and  $A_E$  for Cowley et al. (2003) and Chané et al. (2013), respectively). Below these, in each column, are representations of the expected ion (solid blue line), neutral (dashed red line), and effective ion drift (dotted dashed green line, scaled up by a factor of 2 for clarity) line-of-sight velocities seen from Earth at three different altitude positions within the ionosphere for each model. The three rows align with the first three altitude positions ①, ②, and ③ highlighted in Figure 1a, where prefixes S and A highlight the symmetric and asymmetric models (labeled as S1, S2, S3 and A1, A2, A3). Cowley et al. (2003) provide their modeled subcorotation both in distance from the planet and in co-latitude. Although that model focuses on results using a magnetosphere that includes a current sheet distortion, for ease of comparison, we utilize values from the dipolar magnetic field. This is factored against the rotation rate of the planet here to provide ion velocity (and so follows the model assumption of axisymmetry and alignment between the rotational axis and the magnetic pole of the planet). Chané et al. (2013) show magnetospheric plasma velocity as a two-dimensional map, from which we have estimated the magnetospheric velocity at a range of distances along the dawn and dusk axis of the magnetosphere; comparing this with rigid  $\Omega_2$  velocity at the same distance gives a fraction of sub (or super) corotation. This is then projected onto the planet using the same dipole magnetic field mapping values taken from Cowley et al. (2003).

produced at this altitude. This restricts Pedersen currents to the lower ionosphere ② in Figure 1a, as predicted by Tao et al. (2009).

However, the magnetospheric plasma velocities observed by Galileo (Krupp et al., 2001) and subsequently modeled (Chané et al., 2013) were found to be highly asymmetric, with significant subcorotating plasma throughout the dusk magnetosphere, but regions of both corotating and even supercorotating plasma in the magnetospheric dawn flank. Ground-based observations of ionospheric  $H_3^+$  flows within the ionosphere appear to match these flows, showing strong subcorotation at dusk and over the pole, but localized supercorotation at dawn (Johnson et al., 2017). The right column of Figure 2 provides a cartoon view of how the flows modeled in Chané et al. (2013) would be observed as Doppler-shifted velocities in Jupiter's ionosphere. The ionospheric flows ( $A_V$ ) remain largely subcorotational (blue) except for a localized region of supercorotation at the pole (red), but there is a clear asymmetry in the flows, with weaker dawn and stronger dusk in their subcorotation. Chané et al. (2013) suggest that this results in significant asymmetries in auroral emission ( $A_E$ ), with weakened auroral emission in the dawn-noon sector and enhanced emission on the midnight side (although we note that Ray et al., 2014 predict asymmetric intensities that are almost the exact inverse of these emissions). Chané et al. (2013) do not model Jupiter's neutral atmosphere, but when the asymmetric subcorotation modeled in their study is mapped into

the atmosphere, the equivalent ionospheric flow represents a  $\sim 3$  km/s ion wind shear between dawn and dusk. According to the ion drag modeled in Tao et al. (2009), neutral winds would only vary by up to  $\sim 0.03$  km/s in the  $\sim 5$  hr it takes for the neutrals to rotate between dawn and dusk. Even with a huge enhancement in ion drag, neutral velocities should remain broadly rotationally symmetric.

As a result, while the ion winds are strongly asymmetric in velocity, the neutrals move with the same velocity as in the symmetric case, and the effective ion drift velocity comes from the difference between these two differing flows. At the lowest altitudes (A1) both ions and neutrals again corotate with the planet, producing no effective ion drift. At moderate altitudes (A2), the neutral atmosphere is still affected by other acceleration forces, resulting in a  $k$  factor (here  $k = 0.5$ ). But importantly, this is relative to ion flows rotationally averaged over tens of jovian rotations. The result is an effective ion drift (green) that has enhanced supercorotation at dawn, weak subcorotation over the pole, and very strong subcorotation at dusk. At higher altitudes (A3), neutral winds have moved into full subcorotation with the symmetrically averaged magnetosphere. This effectively removes the breakdown in corotation (as in the symmetric case S3), leaving only asymmetric magnetospheric flows. The resultant line-of-sight effective ion drift velocity consists of two blue-shifted ion winds flowing toward the observer and Sun, representing a strong supercorotation at dawn and subcorotation at dusk. In turn, this provides an effective Pedersen conductivity that allows a Pedersen current to flow from dawn to dusk on both sides of the auroral oval. It suggests that in regions where the neutral atmosphere is dominated by ion drag (i.e.,  $\textcircled{3}$  in Figure 1a), breakdown-in-corotation currents would not close through the ionosphere, but the asymmetric currents associated with asymmetric flows within the magnetosphere could close.

Searching for this hypothesized high-altitude effective ion drift requires a way to remotely measure winds in both the ionosphere and the thermosphere in the same altitude range. We use NIRSpec (McLean et al., 1998), the near-infrared long-slit spectrometer on the Keck II telescope, to simultaneously observe the quadrupole  $\text{H}_2$  and overtone  $\text{H}_3^+$  lines shown by Kita et al. (2018) and Uno et al. (2014) to emit in the  $\sim 700$ – $900$  km altitudinal range. The high spectral resolution of NIRSpec allows us to measure the ion and neutral line-of-sight velocities to examine whether our prediction for the effective ion drift, highlighted in Figure 2 (A3), is representative of what is seen at Jupiter. In Section 2, we describe our reduction and analysis of these observations. In Section 3, we present the resultant measurements of the  $\text{H}_3^+$  ion winds, the  $\text{H}_2$  neutral winds, and the calculated effective line-of-sight ion drift velocities. In Section 4, we discuss the implications of this for Jupiter's aurora, as well as the broader implications for Jupiter's atmosphere and Pedersen currents at other planets, before providing conclusions in Section 5.

## 2. Observation and Data Processing

Observations of Jupiter's auroral region were conducted on 2 June 2017 from 06:23 to 07:40 UTC using Keck's NIRSpec. The echelle position and the cross disperser position were set at 63.9 and 35.6, respectively. From the pole toward the equator, the jovian northern aurora was scanned twice with a long slit aligned east-west, perpendicular to the rotational axis, under a K-band filter. The first scan utilized a  $0.432 \times 24''$  slit and the second a  $0.288 \times 24''$  slit, the latter scaled to the first scan's spectral resolution of  $\sim 25,000$ . The average air mass and seeing of the night were recorded as  $\sim 1.1$  and  $\sim 0.6$ . Jupiter's equatorial diameter was measured  $\sim 40.6''$ , with a sub-Earth latitude of  $\sim -3.098^\circ$ . A total of 38 spectral images, excluding sky frames, were obtained by combining six integrations, each 10 s long. In this study, three echelle orders of emission lines, order 35 (2.177–2.209  $\mu\text{m}$ ), order 36 (2.117–2.148  $\mu\text{m}$ ), and order 37 (2.059–2.090  $\mu\text{m}$ ) were analyzed.

In addition to standard astronomical data reductions, further calibrations are performed to correct skyline wavelength offsets and slit shifts. We follow Johnson et al. (2017) and Stallard et al. (2001) in processing Doppler shifts into line-of-sight velocities, including conversion of reference frames. The spatial effect of asymmetric illumination of the spectral slit is corrected within each spectral position using emission from the preceding and following spectra, allowing us to calculate the estimated spatial effect, following the exact methodology outlined in Johnson et al. (2017). Velocities presented in this study are derived in reference frames with respect to the observer and the rate of planetary rotation, aided by the movement of the magnetic pole. Refer to Supporting Information S1 for more details of the whole process.

## 3. Results

Figure 3 shows the two scans of Jupiter's northern aurora taken on 2 June 2017. In the left column, we show the  $\text{H}_3^+$  emission brightness (Figure 3a), plotted above the measured line-of-sight  $\text{H}_3^+$  (Figure 3b) and  $\text{H}_2$  (Figure 3c)

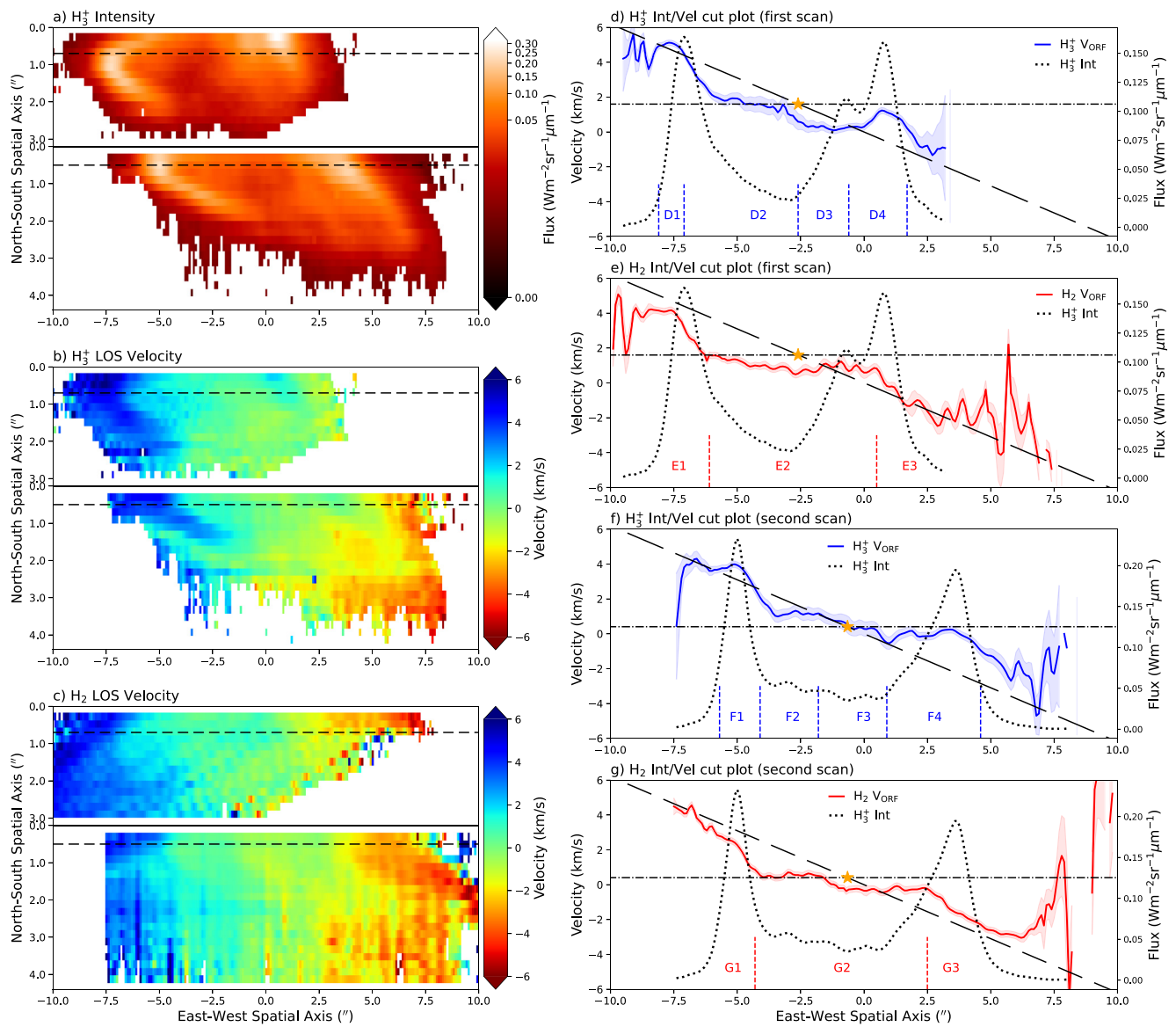


**Figure 3.** Scanning maps and profiles of measured  $H_3^+$  flux,  $H_3^+$  LOS velocity, and  $H_2$  LOS velocity from Jupiter. On the left, the three panels show (a) measured  $H_3^+$  flux, (b)  $H_3^+$  LOS velocity, and (c)  $H_2$  LOS velocity from Jupiter. In the velocity maps, blue and red correspond to the positive and negative velocities, indicating blueshift and redshift, respectively. White shows regions with no data coverage. The planetary center is located at 0 along the east-west spatial axis. The dashed black lines highlight the locations of individual cuts through these maps. We show these cuts in the panels on the right. Each cut provides two sets of 1-D measured values taken from a specific individual spectrum. The first set (d, e) both show the  $H_3^+$  emission, plotted with the ion (blue) and neutral (red) velocities, respectively, for a spectrum taken at 06:28, when the central meridian longitude (CML) was 157. The diagonal dashed line stands for the rotation rate of Jupiter. The dotted dashed line refers to the rotation rate of the magnetic pole. The intercept between the planetary rotation rate and the magnetic pole rotation rate is marked by the orange star. Panels (f, g) show the ion (blue) and neutral (red) velocities, respectively, for a spectrum taken at 06:54, when the CML was 178. The vertical red lines separate regions of interest to better guide the reader.

velocities. We compare with the  $H_3^+$  intensities to show the relative position of these velocities. The  $H_2$  intensity is not shown here, but will be discussed in the later study. On the right, we show plots of line-of-sight velocity and intensity for two specific cuts through these scans. In Figures 3d and 3e, we have plotted a 1-D cut of the ion (blue) and neutral (red) velocity maps, respectively, each cutting through the first scan at a central meridian longitude (CML) of 157 (with positioning, shown as the top horizontal dashed black line in Figures 3a–3c). These are both shown relative to the  $H_3^+$  emission brightness (dotted black line). In Figures 3f and 3g, we show the same plots for the second scan at a CML of 178, notable because the dawn and dusk auroras are located at a similar distance from the center of the planet, with the magnetic pole close to the central meridian. For each cut plot, regions of interest have been labeled to guide the reader.



The main auroral emissions shown in Figure 3a are sharp and bright on the dawn side, but more expanded on the dusk side. Significant emissions are found at the dusk pole. These features are typical for both UV (Grodent, Clarke, Kim, et al., 2003) and  $H_3^+$  (Stallard et al., 2016) images of the northern auroral region. Another region commonly seen in  $H_3^+$  images can also be identified here: a polar darkening focused around the magnetic north pole, akin to the P region identified in Stallard et al. (2016). Surprisingly, no clear darkening is found inside the dawn main emission, associated with the Dark region, one of the main UV polar auroral features (Grodent, Clarke, Waite, et al., 2003), which is also typically seen in the infrared (Stallard et al., 2016).

Figures 3b and 3c show that both the ion and neutral velocities are dominated by the rotation of the planet, resulting in blue-shifted velocities at dawn and red-shifted velocities at dusk. Variations in ion drifts are clear within these maps along the east-west spatial axis, with small-scale details better shown in Figures 3d and 3f. For the first cut, the  $H_3^+$  ions in Figure 3d subcorotate (closer to zero than the dashed line of corotation) across the dawn polar region (D2) and in the dusk aurora (D4), both  $\sim 1.7$  km/s slower relative to the rotation rate. On the dawn side, just equatorward of the main emission oval (D1), the ions supercorotate at a relative velocity of  $\sim 0.4$  km/s. The subcorotation in the dawn polar region (D2) appears stationary with the magnetic pole, suggesting that this region is associated with zero velocities in the inertial frame of surrounding Jupiter. It also implies that this region magnetically maps into the outer magnetosphere or the solar wind, similar to previously observed stagnant ion flows (Stallard et al., 2003). The dusk polar region (D3) generally follows the corotation of the planet, but appears slightly red-shifted, perhaps indicating supercorotation. For the second cut, the ion velocities in Figure 3f are somewhat different, where supercorotation is found inside the auroral peak on the dawn side (F1) at  $\sim 0.8$  km/s. The dawn polar and dusk auroral subcorotations (F2 and F4) are at  $\sim 1.1$  and  $\sim 2.4$  km/s, respectively.  $H_3^+$  in the second scan returns to corotation with the planet near the center of the polar region (F3).

Derived neutral flows poleward of the main emission (E2 and G2), shown in Figures 3e and 3g, appear to be highly symmetric around the magnetic pole (intercept between the planetary rotation rate and the magnetic pole rotation rate), with an almost flat subcorotational (subcorotating at  $\sim 10\%$  full rotation) velocity across the entire polar region (E2 and G2). The neutral velocities transition to corotating with the planet equatorward of the main auroral region (E1, E3 and G1, G3). These velocities match well with the line-of-sight velocity of the north magnetic pole rotating around the planet, similar to the dawn polar ionosphere (D2) described above. The projected velocity of the magnetic pole is shown as a dotted dashed slope, crossing the rotation rate of the planet at the magnetic pole (defined as  $75^\circ\text{N}$  and  $185^\circ\text{W}$  by Grodent, Clarke, Kim, et al. (2003)). Notably, the neutral flows appear to match this polar subcorotation well closer to the aurora, with a significant red shift near the magnetic pole, potentially indicating more complex dynamics. More measurements are needed to fully understand this. At lower latitudes, the neutral velocities appear to smooth out with less clear boundaries, instead producing a linear subcorotation across the entire auroral region.

Despite slightly different magnitudes of the velocities, both scans (ion winds in Figures 3d and 3f, and neutral winds in Figures 3e and 3g) overall show comparable velocity gradients. An apparent contrast between the two scans is that, in Figure 3b, the dawn sector blue shift appears to extend down to  $\sim 2.2''$  in the first scan and only to  $\sim 1.5''$  in the second scan. Similar structures can be found in Figure 3c, where  $H_2$  in the first scan blue shifts across the entire north-south spatial axis but becomes stagnant from  $\sim 1.0''$  to  $\sim 1.4''$  in the second scan. The most likely explanation for these differences is that the changing flow vector of the ionosphere and atmosphere around the offset aurora turns this dawn region from a direction more parallel to the observer's look direction to flowing more perpendicularly, a product of the offset morphology of the aurora. Red-shifted velocities on the dusk sector are not seen to change in the same way, because the auroral morphology in this region is part of the magnetic field "kinked" by subsurface equatorward fields (Connerney et al., 2022; Grodent et al., 2008), resulting in a vector that appears as an approximately straight line toward the observer, much less affected by the changing viewing angles with the rotation of the planet. This difference can be seen in the change in location of the peak  $H_3^+$  brightness shown in Figure 4a.

To understand the ion wind velocities in the neutral reference frame, we subtract the  $H_2$  velocity from the  $H_3^+$  velocity and thus observe line-of-sight effective ion winds for the first time, as shown in Figure 4. Figure 4a remains the same as in Figure 3, except that, for clarity, we have traced the measured location of the peak  $H_3^+$  brightness on both the brightness and velocity maps (solid white). In Figure 4b, the effective ion drift is clearly dominated by two blue-shifted sunward flows in the jovian ionosphere. Notice that the positions of the dawn and dusk blueshifts follow the line of  $H_3^+$  intensity throughout the auroral region, with the dusk side slightly offset equatorward of the main auroral oval.

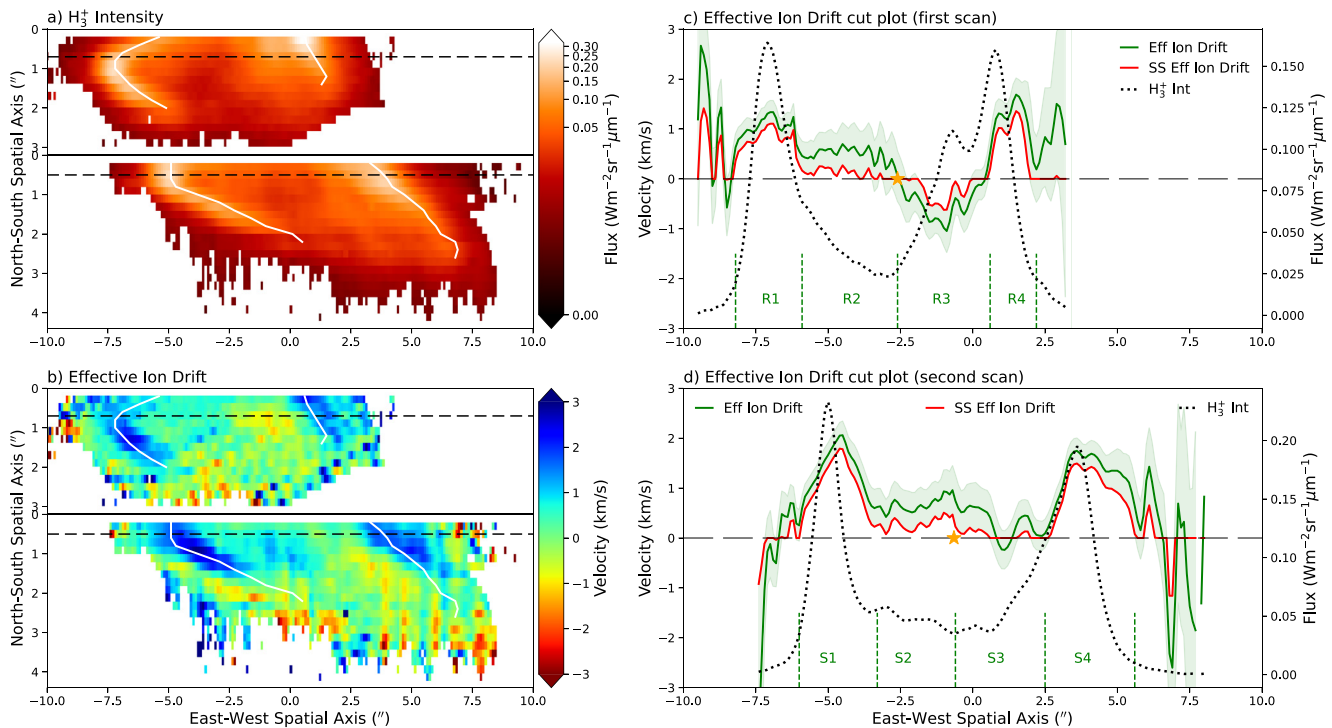


**Figure 4.** Scanning map of measured  $H_3^+$  flux (a), relative velocities between  $H_2$  and  $H_3^+$  (b), and two 1-D cut through of the velocity map (c, d), respectively corresponding to the top and bottom horizontal dashed line in (a and b). (b) Produced by subtracting Figure 3c from Figure 3b. (c, d) The solid green line represents the relative velocity (“Eff ion drift”). The solid red line outlines the same velocity with errors factored in, labeled as the statistically significant effective ion drift (“SS Eff ion drift”). The horizontal dashed line refers to the rotation rate of Jupiter. The two lines mark the peak auroral emissions. All other plotting format remains identical to Figure 3.

Again, to reveal detailed variations, two 1-D cuts of the first and second scan, Figures 4c and 4d, respectively, are produced as in Figure 3. Two strong blue-shifted effective ion drifts are revealed on both the dawn and dusk sides of the planet. Here, the LOS component of Jupiter's rotation rate has been removed, so zero velocities refer to ions corotating with the planet. For the first cut, the wind speed at dawn is  $\sim +1.5$  km/s and at dusk  $\sim +1.8$  km/s, and for the second cut,  $\sim +2.2$  km/s and  $\sim +1.9$  km/s, respectively. The dawn aurora extends across the main emission (R1 and S1), peaking just duskward, and continues across the majority of the dawn polar region (R2 and S2). On the dusk side, another blue shift can be seen duskward of the main emission (R4 and S4), in addition to a small-scale red shift on the dusk side of the polar region (R3 and S3). The entire polar region (R2, R3 and S2, S3) reveals both a blueshift and a redshift between the two auroral arcs, a phenomenon persistent through both auroral scans taken that night. The separation point is close to the magnetic pole (orange star) in the first scan and near the planetary rotation axis (0.0”) in the second scan. Since both the magnetic and the planetary centers are only estimated, we cannot determine whether this is a supercorotation throughout the polar region or a supercorotation turning into a subcorotation on the dawn sector.

Uncertainties in our velocity measurements, in Figure 3, are mainly due to the differing accuracy of correcting instrumental spatial effects. Because of this, interpreting the relevance of flows seen in our effective ion-drift velocity maps is a challenge. In Figure 4, we have highlighted the statistically significant value of the effective ion drift allowed by the calculated uncertainties, meaning that any values along this red line are above our uncertainties and can be confidently discussed. Where the uncertainties cross the zero line (e.g., near the center of the planet in Figure 4c), we set the velocities to zero. The red shift close to the center of the planet in Figure 4c still exists even with uncertainties factored and the flows in regions nearby are now in corotation. In the second scan, a small-scale corotation is noticed in Figure 4d on the dusk side of the polar region, while most of the polar region remains blue-shifted. In Figure 5, we replot the observed effective ion drift shown in Figure 4b along with an adjusted figure showing the statistically significant velocity map, mapping the red line described above, where only flows outside the uncertainty range are included. Clearly, the two blue jets are well above noise and the overall velocity structure remains fairly similar. The blueshift and redshift in the polar region mentioned above

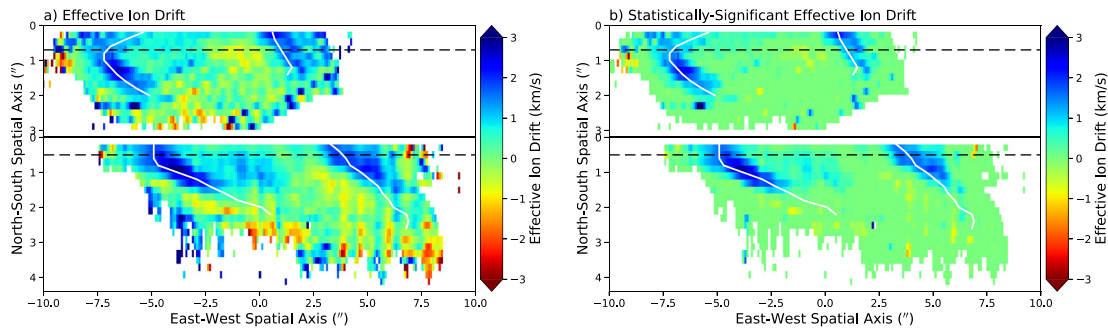


**Figure 5.** Scanning map of measured relative velocities between  $H_2$  and  $H_3^+$  (a) with effects of measurement uncertainties included, and (b), produced by factoring only flows falling outside of error limits in Figure 4b. All other plotting format remains identical to Figure 4.

both rise weakly above the error limit, suggesting complex dynamics of polar flows in addition to the main result of the blue-shifted effective ion drift.

#### 4. Discussion

The  $H_3^+$  ion wind velocities measured in this study are broadly similar to past observations. We observe a subcorotation across the polar region, returning to corotation outside the auroral region, as well as a significant subcorotation on the dusk side, which are all observed by Chaufray et al. (2011), Johnson et al. (2017), and Stallard et al. (2001). We also find a supercorotation on the dawn side of the auroral oval, focused close to the main emission; this was observed by Chaufray et al. (2011) and Johnson et al. (2017), while Stallard et al. (2001) observed a subcorotation on the main emission, with a supercorotation occurring equatorward of the main emission. The dawn polar region appears to be near stagnant with the magnetic pole, in agreement with Stallard et al. (2001), while Johnson et al. (2017) showed stagnation only in the “dark” region close to the dawn main emission. Possibly, Johnson et al. (2017) resolved a significant reduction in emission in this region, while both Stallard et al. (2001) and our result report unreduced emission close to the dawn edge of the polar region.

Our neutral wind measurements for the first time resolve a strong polar vortex that subcorotates inside the main auroral emission. The flows observed by Chaufray et al. (2011) are structure-consistent with the neutral winds measured here. Unfortunately, the uncertainties associated with those observations were so large that it was not possible to distinguish between a full corotation and a zero velocity in the inertial frame. The strong similarity to the velocities presented here perhaps suggests that the uncertainties computed in that study were overestimated. At lower latitudes, the anticyclonic flow of the vortex appears to match a general trend of jovigraphic subcorotation across the entire auroral region, making it harder to pick out the auroral boundary in the neutral velocities. This may indicate that neutrals flowing at lower auroral latitudes are part of a global subcorotation, along lines of equal jovigraphic latitude (rather than jovimagnetic latitude), more like the flows modeled by Bougher et al. (2005). Notably, this shift in velocity across the auroral polar region seems to correlate well with the shift observed by Stallard et al. (2003) in ion velocities, with the “f-DPR” region showing a stagnant close-to-zero rotation in the polar regions at higher latitudes, and the “r-DPR” region showing only moderate subcorotation at lower latitudes. This perhaps indicates that the polar regions within the 1998 data set analyzed by Stallard et al. (2003) may have been following velocities much more like the neutral velocities observed here than the ion winds seen in this study. This again points to abnormal dynamics in the dawn polar region during the observations herein.

We notice that the darkest region in the polar region sits close to the rotational pole, matching the polar emission structure seen in Stallard et al. (2003). This aligns with the location of the lowest effective ion drift. Johnson et al. (2017) see differences in both the dawn polar brightness and ion winds. Assuming similar neutral flows to those observed here during Johnson et al. (2017)’s observations would result in two regions of low effective ion drift, one close the dawn main emission, aligning with the dark “D” region, and the second at the center of the planet aligning with the dark “P” region of that paper. This hints at a potential co-incidence between the effective ion wind velocity and polar auroral brightness across the dawn polar region, perhaps indicating dynamics associated with solar wind as a driver for auroral emission in this region.

Both measured ion and neutral winds broadly match our predictions of the expected flows in the upper ionosphere, based on magnetospheric flows from Chané et al. (2013) and Cowley et al. (2003), respectively. The

observed ion winds agree well with the overall asymmetric magnetospheric flows when mapped onto the planet shown in Figure 2 (A3). The main difference is the broadened dusk subcorotation, which matches past observations (Chaufray et al., 2011; Johnson et al., 2017; Stallard et al., 2001), and may indicate that the strong magnetospheric subcorotation extends closer to the planet at dusk than Chané et al. (2013) predicts. Most notably, our observations of the line-of-sight effective ion drift velocities also appear to match well with our predictions of the effective ion drift in Figure 2 (A3), with two sunward blue-shifted jets on each side of the main auroral region. There are clearly smaller-scale differences between the observed ion winds in the neutral frame and those predicted in Figure 2, which probably originate in both temporal differences and the simplistic mapping used in our predicted winds. In reality, ion winds will closely follow the complex morphology of the auroral emission, whereas the neutral winds are likely forced to circularize in the atmosphere relative to these asymmetric driving ion winds.

#### 4.1. Predictions of Pedersen Currents Driven by the Observed Flows

Our observed effective ion drifts show that the upper atmosphere is clearly more dynamic than predicted axisymmetric models, due to the asymmetry in the magnetospheric flows and the extended multiday lag between ion and neutral winds. This means that at altitudes with significant true Pedersen conductivity ( $\Sigma_p$ , as shown in Figure 1), the ionosphere can carry a Pedersen current perpendicular to the observed effective ion drift (i.e., there is a significant effective Pedersen conductivity  $\Sigma_p^*$ ). The regions where the observed effective ion drift velocities are strongest, where the line-of-sight ion wind points directly toward or away from Earth, are the regions of the planet where the magnetic field ranges between 4 and 8 G (Connerney et al., 2022). In these regions, the Pedersen conductive layer reaches up to  $\sim 550$  km, only narrowly overlapping with the emission column of both  $H_2$  and  $H_3^+$  observed here. However, the fundamental  $H_3^+$  emission observed by Johnson et al. (2017) and Stallard et al. (2001) peaks close to this altitude (Kita et al., 2018), a region in alignment with the magnetospheric velocity  $\omega_m$  (as shown in Figures 1a and 1b), and where the neutral atmosphere is strongly coupled with the symmetric ionospheric velocity ( $k \sim 0.85$ ; Tao et al., 2009).

The  $H_2$  emission observed here peaks above the true Pedersen conductivity boundary, and there are no measurements of the underlying auroral atmosphere. However, Figure 1c highlights neutral velocities that vary more slowly with depth, so the only significant change within the neutral atmosphere will be that the symmetric flows observed here may weaken deeper in the atmosphere. Indeed, models predict that the neutral atmosphere will be dominated by the underlying internal rotational velocity ( $\Omega_j$ ) rather than the magnetospheric subcorotation ( $\omega_m$ ) only deep in the ionosphere (with Tao et al., 2009 predicting  $k = 0.5$  at  $\sim 430$  km and  $k = 0.25$  at  $\sim 350$  km), where the ion drag no longer dominates the acceleration of the neutral atmosphere. The effective ion drift observed in  $H_3^+$  emission at altitudes of  $\sim 800$  km (as observed here) is thus likely to be broadly representative of effective ion flows between  $\sim 400$ – $600$  km, allowing this entire column of the ionosphere to carry asymmetric Pedersen currents. Even below this region, our prediction was that significant asymmetries would remain even in the deepest ionospheric layer, as highlighted in Figure 2 (A2).

As a result, the observed effective ion drifts imply significant asymmetric Pedersen currents flowing within the upper atmosphere, dominating above the region where the breakdown in corotation is predicted to drive currents. In Figure 6a, we provide a cartoon highlighting the observed effective ion drift, along with the likely perpendicular Pedersen currents that these flows suggest, mapped into Jupiter's northern auroral oval, including both the clearly detected sunward effective ion drift jets measured well above the calculated uncertainties (solid lines) and those ion flows closer to the calculated uncertainties (dashed lines).

Figure 6b highlights a simplified version of this current system, including only the sunward effective ion drifts (along with closing flows over the pole) and circularizing the auroral morphology, aligned with the predicted ionospheric currents that result from Jupiter's cross-tail current system. Focusing initially only on two strong sunward flows shown in Figure 5b, each of the blue-shifted jets moves ions toward the Sun through the upwardly directed magnetic field, resulting in Pedersen currents that flow from dawn to dusk. These Pedersen currents must close in the surrounding magnetosphere, in turn implying that the ionosphere experiences a strong downward current associated with these Pedersen currents near the main auroral emission and an upward current further to the dusk of each auroral arc (poleward of the main aurora on the dawn side and equatorward of the main aurora on the dusk side). Assuming that these sunward flows are parts of a twin-cell vortex with antisunward flows over the pole, like the Dungey cycle at Earth, they would produce a system of Pedersen currents that appears very similar

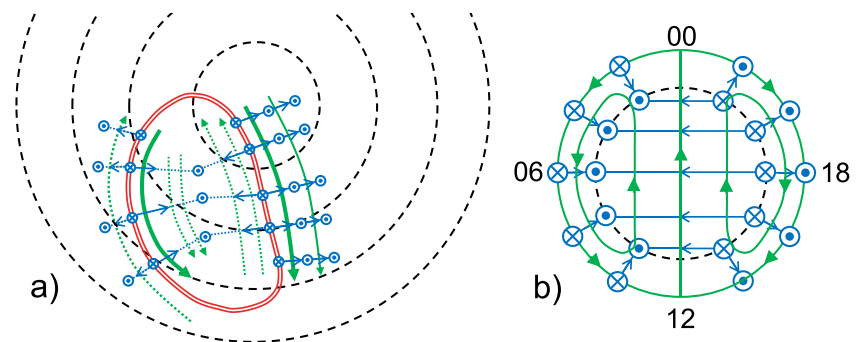


**Figure 6.** A cartoon diagram highlighting the predicted Pedersen currents with Jupiter's upper ionosphere. On the left, we show the observed line-of-sight effective ion drift in the neutral frame (solid green arrow line for clear flows and dotted green arrow line where the observed flows are close in scale to the ion wind error), plotted relative to the  $H_3^+$  peak auroral emission (double solid red line). At altitudes where there is significant true Pedersen conductivity, these relative flows will drive perpendicular Pedersen currents (solid blue through regions with certain flows and dotted blue through regions with dotted green ion flows). These currents are the atmospheric manifestation of a current circuit that closes along magnetic field lines into the magnetosphere and so must flow into and out of the atmosphere at points where the Pedersen currents diverge and converge (blue crosses and dots within circles, respectively). These are contextualized by the location of the main auroral emission (double solid red line). On the right, for comparison, is a simplified diagram showing the expected Pedersen currents flowing through the ionosphere, closing Jupiter's magnetospheric partial ring current system, as described in Khurana (2001). The cross-tail current is in the opposite direction of Earth's, as is the direction of the magnetic field, so that while the Pedersen current flows in the opposite direction to Earth, the  $\vec{E} \times \vec{B}$  flows are the same, sunward along the auroral flanks and antisunward across the pole.

to the region 1 and 2 currents observed at Earth, similarly driven by the closing of the cross-tail currents into the atmosphere. The upper ionosphere thus allows the closing of the “partial ring current” that flows from dawn to dusk within Jupiter's magnetotail (Khurana, 2001).

Although the strongest flows shown in Figure 5b allow us to see the broadest current system highlighted in Figure 6b, more weakly and more complex flow structures are also observed and are more clearly shown in Figure 5a. These flows appear to produce extended flow structures within the polar region. The dawn polar region is blue-shifted, suggesting supercorotation across a broader region of the magnetosphere. There are also two localized regions of the antisunward flow. The first, in the dusk polar region of both scans, perhaps suggests a Dungey-like return flow focused on the dusk side of the auroral region. A second antisunward flow appears in the second scan, in the equatorial dawn flank of the aurora, perhaps hinting at a more complex flow structure. These ion winds could potentially produce a series of additional Pedersen currents, as shown in Figure 6a (dashed lines).

Finally, in predicting expected ion flows in the lowest layers of the ionosphere (A2 in Figure 2), we suggested that the magnetospheric flows modeled by Chané et al. (2013) should produce significant dawn supercorotations even at depth. Their simulation predicted weaker main emission in the pre-noon sector, but such emission asymmetries are not observed in the  $H_3^+$  auroral brightness here, and are not consistently observed in past measurements of the main auroral emission either the infrared (e.g., Johnson et al., 2017; Stallard et al., 2016) or ultraviolet aurora (e.g., Bonfond et al., 2015). Our observation has revealed that a large column of the ionosphere (perhaps 400–600 km) has effective Pedersen conductivity dominated by asymmetric flows, allowing only asymmetric Pedersen currents to move through the ionosphere. As these asymmetric currents close, the asymmetric component within the electric field will be reduced at that altitude, propagating into the underlying ionosphere. The deeper into the ionosphere the imposed magnetospheric electric current penetrates, the more the asymmetric component of that electric field will have been closed through the ionosphere. We speculate that this ongoing closure of the asymmetric electric field with depth acts to draw down the imposed asymmetries, so that symmetric electric field components dominate at deeper layers. These symmetric components cannot close until they penetrate to a depth where the neutral atmosphere is no longer dominated by the ion drag. If the extended closure of asymmetric currents across the deep column of the ionosphere drains the majority of the asymmetric electric field, the final breakdown-in-corotation at the base of the ionosphere would occur with a purely symmetric electric field, the only component of the electric field shielded from closure within the upper ionosphere by moving with the neutral atmosphere in these layers. This would suggest that the deepest layers of the ionosphere

would better resemble the S2 region within Figure 2, producing a broadly axisymmetric auroral current from the breakdown in corotation.

#### 4.2. Potential Implications of Asymmetric Flows to Our Understanding of Jupiter's Aurora

As highlighted in the Introduction, past predictions from models of the magnetospheric flows closing in the atmosphere have struggled to predict the observed auroral morphology and current systems, particularly the recent measurements made by the Juno spacecraft. The discovery of a layer in Jupiter's ionosphere that is able to conduct only asymmetric or temporally variable currents opens up the potential to resolve many of these conflicting measurements.

Simultaneous auroral observations of the H and H<sub>2</sub> ultraviolet emission and H<sub>3</sub><sup>+</sup> infrared emission using Juno's UVS and JIRAM instruments reveal starkly different auroral displays (Gérard et al., 2018), especially on the dusk side of the main emission. In the infrared, the dusk H<sub>3</sub><sup>+</sup> is highly striated, with numerous thin arcs of emission, none of which dominate. On the contrary, the UV emission is dominated by a single sharply defined arc of emission, but this is typically partially obscured by weaker background emission. This broadened background region exactly aligns with the striated arcs observed in the H<sub>3</sub><sup>+</sup>. The bright UV arc has a high color ratio, indicating that it is produced well below the homopause, with hydrocarbons absorbing the emission as it radiates outward. Surrounding this, the weak emission that matches with the H<sub>3</sub><sup>+</sup> striated emission has a very low color ratio, indicating little hydrocarbon absorption. This region consists of relatively low energy flux particle precipitation, ionizing and exciting only the upper atmosphere. UV and H<sub>3</sub><sup>+</sup> emissions typically occur within broadly overlapping regions of the atmosphere, with both dominated by emission from their lowest respective layers, falling away with altitude. However, UV emission is dominated by emission in an altitude layer below the homopause, while protonation with hydrocarbons destroys H<sub>3</sub><sup>+</sup> below the homopause. Tao et al. (2011) place this UV peak at 350 km, where the H<sub>3</sub><sup>+</sup> emission is three orders of magnitude weaker at this altitude than at the H<sub>3</sub><sup>+</sup> peak closer to 600 km. The localized H<sub>3</sub><sup>+</sup> emission structure is dominated by H<sub>3</sub><sup>+</sup> density, rather than temperature changes, so that UV and H<sub>3</sub><sup>+</sup> emission structure is typically similar, apart from the high color ratio UV emission (Stallard et al., 2016). As a result, UV emission is produced through a combination of both excitation by the same drivers that produce ionization that drives the H<sub>3</sub><sup>+</sup> emission and high energy precipitation that produces a high color ratio UV emission and only relatively weak H<sub>3</sub><sup>+</sup> emission (Tao et al., 2011).

Notably, these two different forms of emission align well with the Zone-I and Zone-II auroras observed by Juno in situ measurements of auroral currents (Mauk et al., 2020). While both Zone-I and Zone-II have significant broadband energy distributions, suggesting strong wave-particle interactions, they are separated by the preferential direction of the currents within them. Zone-I, which aligns with the narrow higher UV color ratio auroral emissions, contains primarily upward currents. Zone-II, which aligns with lower UV color ratios and bright striated H<sub>3</sub><sup>+</sup> emissions, is characterized by larger regions of bidirectional acceleration processes.

This strongly suggests that Zone-II emission occurs in a region dominated by relatively low-energy particle precipitation into the upper ionosphere, above the homopause. Since past models of the breakdown-in-corotation aurora predict strong auroral emissions to only be associated with the upward currents on the inner edge of these magnetospheric currents (e.g., Cowley et al., 2003; Nichols & Cowley, 2022), given the association with Zone-II aurora, it is unlikely the H<sub>3</sub><sup>+</sup> auroral arcs could originate from this breakdown in corotation, even if the breakdown was fragmented into steps at larger distances from the planet. As shown in Figure 6, this auroral emission is dawnward of the observed sunward flows, strongly implying that within the asymmetric current system, this is a region of downward currents. It is unlikely that such downward currents could drive strong particle precipitation, since the strongest auroral emissions should result from upward currents producing downward accelerated electrons, which would produce bright auroral emission duskward of the blue-shifted sunward jets, clearly not observed in the H<sub>3</sub><sup>+</sup> emission. This implies that striated H<sub>3</sub><sup>+</sup> emissions are driven by wave-particle interactions above the planet, as has been suggested by Juno observations (Mauk et al., 2020).

In contrast, Zone-I emission penetrates through the upper ionosphere, resulting in only weak ionization in that layer, with high UV color ratios implying ionization peaks well below the homopause. Comparing the models of ion drag (Tao et al., 2009) and UV emission altitude (Tao et al., 2011) suggests that the main UV emission typically penetrates deep enough (<300 km) to reach layers where ion drag ( $F_i$ ) is only a weak component of the combined atmospheric forces ( $F_T$ ), as shown in Figure 1d. The neutral atmosphere is decoupled from the ionosphere in this

layer, allowing the symmetric breakdown-in-corotation flows to produce an effective Pedersen conductivity and allowing Pedersen currents to close these currents from the magnetosphere. Notably, Zone-I is the only region dominated by upward currents, aligning directly with the prediction from modeling that steady-state continuous upward currents from the breakdown in corotation are a significant driver of bright UV emission (Cowley et al., 2003). This would suggest that high-energy particle precipitation from the upward breakdown-in-corotation currents produces narrow, bright, and high color ratio UV emissions, interspersed between downward currents associated with the asymmetric magnetospheric flows, resulting in interlaced upward and downward currents throughout the auroral region, as observed by Juno (Mauk et al., 2020).

The interaction of upward and downward currents is likely to be highly complex, especially given the localized variations in magnetospheric flows and the misalignment between ionospheric and neutral flows. This helps explain the dawn-dusk differences observed. When decoupling the  $H_3^+$  auroral emission from the requirement of being driven by the breakdown in corotation, the stark brightness differences between dawn and dusk result from changing wave-particle interactions rather than steady-state continuous currents. These Zone-II aurora also drive asymmetries in the UV emission, due to the significant area these weaker low color ratio UV emissions extend over. At dawn, supercorotational flows are very narrowly confined, but at dusk strong subcorotation spreads outward, with the differential shearing of plasma spreading out along the dusk flank shaped by the influence of the Solar Wind (Kivelson & Southwood, 2005), resulting in very different wave-particle interactions associated with these two regions.

Jupiter's main auroral emission is also strongly enhanced with the arrival of compressed Solar Wind to the magnetosphere (Baron et al., 1996; Clarke et al., 2009; Nichols, Clarke, et al., 2009; Nichols et al., 2007; Yao et al., 2022), in direct contrast with the predictions of models of corotation breakdown. These predict a weaker aurora in response to the solar wind compression, owing to the compressed magnetosphere; as ions should be pushed into smaller and faster-moving orbits, causing a decrease in the resultant currents (Cowley & Bunce, 2001, 2003; Southwood & Kivelson, 2001). However, because of the very slow ion drag, any change to the location or strength of ion flows, whether faster or slower, would result in a significant effective ion drift, since the neutral winds would be slow to catch up to short-term ion wind flows, allowing Pedersen currents to close across the entire column of the ionosphere.

An alternative source for enhanced precipitation comes from the prediction that solar wind compressions are expected to enhance asymmetric flows within the magnetosphere (Chané et al., 2017). Recent comparisons between the dawn UV auroral brightness observed by the Hubble Space Telescope and the simultaneous magnitude of the dawn side magnetospheric equatorial radial current show these are highly correlated (Nichols & Cowley, 2022), suggesting that the breakdown-in-corotation currents rather than currents associated with asymmetric flows are the main driver of these differences. With rapidly changing ion winds during compression, the breakdown-in-corotation Pedersen currents will produce effective ion winds across the entire ionospheric column, potentially driving currents through the upper ionosphere and enhancing  $H_3^+$  emission along the main oval. However, investigations of the morphology of auroral enhancements during solar wind compression by Dunn et al. (2020) highlight that while the dawn aurora observed by Nichols and Cowley (2022) is enhanced almost immediately, the dusk region is only significantly enhanced on the second day after the arrival of the compression, at which time, the dusk UV emission contains multiple arcs of emission. This suggests both breakdown-in-corotation and asymmetric magnetospheric flows are important to auroral enhancements, either through enhanced wave-particle interactions or the driving of enhanced field-aligned currents associated with asymmetric currents. Only through observations of the changing field-aligned and Pedersen currents during compressional solar wind events will we be able to assess what drives how the solar wind forces Jupiter's coupled atmosphere and magnetosphere to generate such bright auroral emissions.

This result highlights that any other source of variable magnetospheric flows, either spatially or temporally on a timescale of less than tens of days, will also produce significant effective ion drifts across the entire ionosphere, allowing high effective Pedersen conductivities and closing Pedersen currents across most of the ionosphere. As the magnetosphere of Jupiter is replete with potential sources of such complexity, including magnetospheric dynamics from plasma lost in the tail, changing solar wind conditions, or volcanism from Io, it is likely that variability in the magnetosphere will inevitably drive both wave-particle instabilities and enhanced currents flowing through and thus into the ionosphere.

### 4.3. Importance of Coupling Between the Ionosphere and Neutral Atmosphere

Our observations have highlighted the importance of neutral atmospheric flows for a fuller understanding of magnetosphere-ionosphere coupling. While ion drags can strongly mitigate the effective Pedersen conductivity of most of the ionosphere by forcing the neutral atmosphere to corotate with the ionosphere (and ultimately, the magnetosphere), the acceleration from ion drag is very slow. The measurements of these flows in this study are very broad-scale; therefore, the localized striated arcs of emission seen in Juno observations of the aurora cannot be resolved in our ground-based observations, and so equally complex variations in either ion or neutral winds would also be obscured.

The likely morphology of the neutral atmospheric vortex produced by the ion drag is unknown beyond the observations discussed here. Most models highlight that neutral momentum is transferred meridionally, with both Achilleos et al. (2001) and Millward et al. (2005) showing a narrow ion wind around the main auroral emission driving a neutral vortex toward the magnetic pole, offset from the rotational pole. Unfortunately, these models rely upon a circular auroral oval and cannot provide insight into the shape of the neutral vortex when driven by the highly asymmetric morphology of Jupiter's northern magnetic field and aurora. Bougher et al. (2005) model an asymmetric auroral morphology and imposed ion wind structure, but this model predicts that Coriolis forces drive the winds westward, resulting in a vortex focused on the rotational pole, rather than the magnetic pole. This is in direct contrast to the predictions of Achilleos et al. (2001) and Millward et al. (2005), as well as our observations. As a result, the final neutral vortex morphology is poorly constrained by modeling. However, there is evidence within our observations that the shapes of ion and neutral flows do not match well across the auroral region, with lower latitude regions seeing the region of subcorotating neutral winds extending beyond the main auroral region. Notably, even in altitude regions where the ion drag dominates, other neutral interactions can still change the overall velocity structure (Tao et al., 2009), so the ion drag cannot perfectly shape the neutral atmosphere. Only detailed asymmetric modeling of these drivers can measure the extent to which the neutral atmosphere nullifies magnetospheric currents with changing altitudes.

Regions where atmospheric flows do not match with magnetospheric driving will cause currents to be driven out into the magnetosphere, in turn changing the dynamics within the magnetosphere. Smith and Aylward (2009) highlighted how meridional advection smooths thermospheric flows, driving feedback into the magnetosphere, and changing the angular velocity of the magnetospheric plasma. A more powerful example of this feedback can be found at Saturn, where recent observations of the auroral ion winds there have shown that a twin cell vortex within Saturn's atmosphere is the source of the radio auroral pulse, and its associated UV and  $H_3^+$  emission (Chowdhury et al., 2022). This aurora, approximately 50% of the total auroral brightness, is driven by atmospheric dynamics, driving currents that are then forced out into the surrounding magnetosphere.

Ion drag forcing of Earth's thermosphere has been shown to produce complex disturbed conditions across the polar region, with localized regions of heating and cooling and associated localized cyclonic and anticyclonic vortices (Walterscheid & Crowley, 2015). Similar dynamics at Jupiter would produce significant complexity in the effective Pedersen conductivity across the auroral region, and could potentially drive currents out into the magnetosphere. Smith (2013) has shown that weather systems within the stratosphere that have scale sizes greater than  $\sim 100$  km can generate electric fields that penetrate almost unmodified across the whole thermosphere, heating this region and probably then driving interactions out into the magnetosphere.

Jupiter's northern and southern auroral regions map into very different atmospheric locations, with the highly asymmetric northern auroral oval being more offset from the rotational pole than the more circularized southern auroral oval. As a result, the morphology and strength of the neutral atmospheric vortex will likely differ in each hemisphere. This may result in interhemispheric currents between the two auroral regions, driven by differential neutral flows in each hemisphere. Therefore, a dynamic and complex neutral atmosphere could drive significant asymmetries between poles, which have been observed in the electric currents at Jupiter (Kotsiaros et al., 2019) and in the auroral emissions at Saturn (Nichols, Badman, et al., 2009). Such interhemispheric currents could potentially also be an additional source of the switching between upward and downward currents observed above the auroral region (Mauk et al., 2020).

The driving of the neutral atmosphere into a rotationally symmetric vortex suggests that the aurora is able to slowly load the atmosphere with momentum, and this has broader implications for Jupiter's lower atmosphere. Recent measurements of neutral wind velocities within the upper stratosphere (around 0.1 mbar; approximately



four orders of magnitude deeper in pressure than our measurements) have also discovered a vortex flow  $\sim 1/3$  the velocity of the magnetosphere (i.e.,  $k = 1/3$ ) within Jupiter's southern auroral region (Cavalié et al., 2021). This seems to conflict with past models of Jupiter's upper atmosphere that show full corotation at much higher altitudes, but this is the result of the boundary conditions of these models being set much higher in the atmosphere: corotation is assumed as a lower boundary condition at 0.01 mbar in Tao et al. (2009), at 0.001 mbar in Achilleos et al. (1998), and at 0.02 mbar in Bougher et al. (2005), for instance. These models may have significantly overestimated the effective Pedersen conductivity in the lowest regions of the ionosphere, potentially reducing the strength of field-aligned currents associated with corotation breakdown, even at the ionospheric base.

This suggests that the flywheel motion of the thermospheric vortex, built up over years, may extend deep into Jupiter's stratosphere. UV images of stratospheric aerosols made by Cassini revealed the "Great Dark Spot," an atmospheric vortex that formed over the northern auroral region, lasting several months (Porco et al., 2003). The vortex formed at a depth of  $\sim 20$  mbar (Banfield et al., 1998) directly over the northern auroral region, circulating clockwise (i.e., in subcorotation) against the prevailing counterclockwise rotation of the circumpolar vortex. It was held in place for several months before being quickly destroyed by the very strong shear winds in that region (Porco et al., 2003). This vortex must be associated in some way with the aurora, since other features in this layer move quickly relative to System III rotation rate. Given the direct alignment of this vortex with the main auroral oval and the clockwise rotation matching with the subcorotation seen at higher altitudes, we speculate that this feature represents the deepest extent of an atmospheric vortex originating within the thermosphere, able to drive this region of the stratosphere only some of the time. This linking between the stratosphere and magnetosphere is likely to be complex with significant feedback.

#### 4.4. Implications for Other Planets

At Earth, thermospheric flows are typically not considered when discussing the aurora, but measurements of neutral winds have shown these to be 10% of ion wind velocities in simultaneous measurements at the peak Pedersen layer (Sangalli et al., 2009). Statistical comparisons of ion and neutral winds in thousands of individual measurements by Thayer (2000) have shown that while ion winds peak around 1 km/s and neutrals are often close to 0 km/s, there is a clear tail in the neutral wind distribution where neutrals move at speeds up to 1 km/s, while ion winds reach speeds of 2 km/s. This suggests that neutrals are able to flow at velocities of up to 50% of ion winds, halving the effective ion drift and the resultant Pedersen currents during these events. Indeed, when modeling the energy deposition driven by these auroras, Thayer (2000) predicted that the acceleration of neutrals into motion alongside ions during quieter periods would reduce auroral energy deposition by  $\sim 20\%$ , but during more active periods, energy deposition would decrease by 30%–50%. Thayer (2000) is clear about the cause: "the reduction [...] in amount of energy transferred into the ionosphere-thermosphere system [...] is attributed to the motion of the neutral gas affecting the current distribution in the E region, such that less electrical energy is needed to power the magnetic field lines through the ionosphere." This reduction is a different view of the same "effective Pedersen conductivity" discussed in past Jupiter papers, and the effective ion drift discussed here, with reduced Pedersen currents producing a reduced Joule heating. However, there remain very limited discussions within the Earth community of potential feedback from the thermosphere back into the magnetosphere. Very recent models have begun to include two-way interactions between the thermosphere and magnetosphere, and have highlighted that coupling with the thermosphere directly impacts how magnetospheric currents are closed through the high-latitude ionosphere (Burleigh et al., 2022) and may be a source of significant hemispheric asymmetries in cross-polar-cap potential, hemispheric power, and ion convection at Earth (Hong et al., 2023). Notably, as with Jupiter, the extent to which the thermosphere changes the magnetosphere-ionosphere coupling varies with the position on the planet, with Thayer (2000) predicting stronger effects for longer auroral events, with that reduction occurring most strongly in the dawn sector. Perhaps, as with Jupiter, the thermosphere has a significant and sometimes dominant effect on the ionospheric currents, a potential gap in our understanding that requires more investigation.

Similar neutral wind modulation of the ionospheric currents is also likely to be of great importance at other outer planets. Most obviously, Saturn's recently discovered "weather-driven" aurora represents an extreme manifestation of this effect (Chowdhury et al., 2022), where neutral winds driven from beneath Saturn's ionosphere drive the neutral thermosphere faster than the ionosphere, generating, rather than carrying, auroral Pedersen currents. However, while these neutral flows generate approximately half of Saturn's aurora, it is likely that the modulating

effect of the neutral atmosphere also has a significant effect on those currents associated with magnetospheric flows. Measurements of ion winds at Saturn have revealed very strong subcorotation across the entire auroral pole (Stallard et al., 2004). Past modeling has failed to fully explain the generation of the magnetospherically generated aurora at Saturn, since currents from the breakdown in corotation near Enceladus are too weak to generate auroral currents (Cowley & Bunce, 2003) and the main auroral emissions occur well equatorward of the open field-line boundary (Bunce et al., 2008). Thermospheric neutrals at Saturn are likely driven to move with the Keplerian magnetospheric velocities, as at Jupiter, resulting in layers of the ionosphere that are only able to close currents associated with the significant asymmetric magnetospheric ion flows observed at Saturn (Kane et al., 2020). Because of the co-location of the rotational and magnetic poles at Saturn, the resultant thermospheric vortices are likely to be more stable and may drive even more energy into the lower polar atmosphere. Future investigations into the magnetospherically generated aurora at Saturn should investigate these currents in the context of effective ion drifts and Pedersen currents associated with an axisymmetric thermospheric vortex. For Uranus and Neptune, the effects of neutral flows may be even more important. The magnetic poles and thus the auroras occur within the equatorial regions of ice giants, where tropospheric winds have significant shears with latitude. If these tropospheric winds are able to drive matching thermospheric winds, as has been suggested in Saturn's equatorial region (Khurana et al., 2018), there may well be significant thermospheric neutral winds that flow across the auroral region, potentially producing complex currents that could modulate or even drive aurora.

Overall, this discovery reveals that understanding the coupling between the magnetosphere and ionosphere of an astronomical body is no longer enough to explain the auroral currents produced. A detailed understanding of the coupling between the thermosphere and the underlying atmosphere is also needed, as thermospheric flows can strongly modulate how magnetospheric flows are closed within that object.

## 5. Conclusion

We have observed for the first time line-of-sight  $H_3^+$  ion winds in the reference frame of  $H_2$  neutral flows in Jupiter's infrared aurora.  $H_3^+$  velocities measured in this study reveal a supercorotation in the auroral oval at dawn, a subcorotation in the polar region, a significant subcorotation at dusk, and a corotation outside the auroral region, broadly consistent with past observations (Chaufray et al., 2011; Johnson et al., 2017; Stallard et al., 2001) and model predictions of asymmetric magnetospheric flows (Chané et al., 2013). The observed neutral flows are the first to resolve thermospheric dynamics at Jupiter, revealing a significant subcorotation within the auroral region, a symmetric anticyclonic vortex driven by ion drag forces accelerating the thermosphere over multiple Jupiter rotations. By subtracting the  $H_2$  velocity from the  $H_3^+$  velocity, line-of-sight effective ion drifts are produced, measuring the ion winds in the reference frame of the neutral atmosphere. These reveal that the effective ion drift in the upper ionosphere (peaking close to  $\sim 800$  km) is dominated by two sunward blue-shifted jets associated with the dawn and dusk main auroral region, with each jet offset to the dusk side of the main auroral emission.

Based upon previous models (Tao et al., 2009), these flows are predicted to overlap with the true Pedersen conductivity layer (which extends across the ionosphere as high as  $\sim 400$ – $600$  km), and so the observed effective ion drifts imply strong Pedersen currents flowing within the upper atmosphere closing asymmetric currents within the magnetosphere. This is in contrast to symmetric breakdown-in-corotation currents, which are modeled to close in the deepest layers of the ionosphere. This implies two significantly different regions of the ionosphere: (a) a deep layer where the thermosphere is dominated by neutral forces, in which symmetric breakdown-in-corotation currents are able to close, and (b) a higher layer where ion drag forces dominate the thermosphere so that the neutral atmosphere moves in a vortex driven by the average magnetospheric flow velocity across multiple planetary rotations. Here, breakdown-in-corotation currents cannot close because the neutral atmosphere moves with the average breakdown-in-corotation velocity, preventing Pedersen currents from forming. However, asymmetric flows in the magnetosphere provide significant shears in the ion wind velocities, so that relative to the neutral atmosphere, Pedersen currents flowing from dawn to dusk allow the closing of the “partial ring current” that flows from dawn to dusk within Jupiter's magnetotail (Khurana, 2001), along with any other asymmetric magnetospheric flows.

This layered ionosphere potentially helps explain several apparent incongruities in recent observations of Jupiter's aurora.  $H_3^+$  emission appears to be dominated by ionization of precipitating particles accelerated by wave-particle interactions, rather than steady-state currents. These auroras are highly asymmetric and extend over a wide range of magnetic mappings, including emission from both the equatorward diffuse aurora and the poleward Zone-II

aurora observed during the Juno flyby (Mauk et al., 2020). A significant amount of UV emission comes from this same source, but an additional narrow arc of broadly symmetric emission penetrates below the homopause, resulting in higher levels of hydrocarbon absorption (i.e., a higher color ratio) in the UV emission and the destruction of any  $\text{H}_3^+$  generated by this more energetic precipitation. This narrow UV main aurora closely aligns with the Zone-I aurora observed during the Juno flyby (Mauk et al., 2020), dominated by primarily downward electron acceleration and therefore upward currents. These are located in a region where the breakdown-in-corotation Birkeland currents are predicted to be upward (e.g., Cowley et al., 2003). Our measurements suggest that the peak  $\text{H}_3^+$  auroral emission on both dawn and dusk are located where asymmetric Birkeland currents associated with dawn-to-dusk Pedersen currents will flow downward, strongly implying that the Zone-I aurora are directly associated with the breakdown-in-corotation and specifically not asymmetric Birkeland currents. In addition, past modeling has suggested that solar wind compressions should generally reduce auroral emissions. However, the changing location and strength of breakdown-in-corotation flow in the magnetosphere will occur far faster than the neutral atmosphere can be accelerated by ion drag, driving significant effective ion drift throughout the ionosphere and allowing significant Pedersen closing currents to form.

Our detection of a strong thermospheric vortex also appears to link with past measurements of similarly directed vortices deeper in the atmosphere, suggesting that momentum from the magnetosphere is a significant driver of neutral flows not only within the thermosphere but also to a considerable depth. There remains a clear gap between the detailed measurements made both here and in other studies, and the models of the magnetosphere-ionosphere-atmosphere coupling system. Future modeling that includes the asymmetric flows of the magnetosphere, the asymmetric shape of Jupiter's surface magnetic field, and a much deeper column of the atmosphere down into the stratosphere are all needed to properly assess the implications of the results presented here.

Finally, we have demonstrated the crucial role of Jupiter's neutral thermosphere in understanding the generation of auroras at Jupiter. It is essential for follow-up observations that can better constrain the variability of both ion and neutral flows, as well as to link these winds with dynamics in both the surrounding magnetosphere and underlying atmosphere. The implications of our results also highlight the potential importance of neutral dynamics for terrestrial and other planetary auroras; we hope that these measurements will help open up a broader discussion about the importance of ionosphere-atmosphere interactions for auroral studies in all planets.

## Data Availability Statement

The data used in this study are publicly available at the Keck Observatory Archive (KOA, <http://koa.ipac.caltech.edu/cgi-bin/KOA/nph-KOAligin>), which is operated by the W. M. Keck Observatory and the NASA Exoplanet Science Institute (NExSci), under contract with the National Aeronautics and Space Administration.

## References

- Achilleos, N., Miller, S., Prangé, R., Millward, G., & Dougherty, M. K. (2001). A dynamical model of Jupiter's auroral electrojet. *New Journal of Physics*, 3(1), 3. <https://doi.org/10.1088/1367-2630/3/1/303>
- Achilleos, N., Miller, S., Tennyson, J., Aylward, A. D., Mueller-Wodarg, I., & Rees, D. (1998). JIM: A time-dependent, three-dimensional model of Jupiter's thermosphere and ionosphere. *Journal of Geophysical Research*, 103(E9), 20089–20112. <https://doi.org/10.1029/98JE00947>
- Banfield, D., Conrath, B. J., Gierasch, P. J., Nicholson, P. D., & Matthews, K. (1998). Near-IR spectrophotometry of jovian aerosols—Meridional and vertical distributions. *Icarus*, 134(1), 11–23. <https://doi.org/10.1006/icar.1998.5942>
- Baron, R. L., Owen, T., Connerney, J. E. P., Satoh, T., & Harrington, J. (1996). Solar wind control of Jupiter's  $\text{H}_3^+$  Auroras. *Icarus*, 120(2), 437–442. <https://doi.org/10.1006/icar.1996.0063>
- Bonfond, B., Gustin, J., Gérard, J. C., Grodent, D., Radioti, A., Palmaerts, B., et al. (2015). The far-ultraviolet main auroral emission at Jupiter—Part I: Dawn-dusk brightness asymmetries. *Annales Geophysicae*, 33(10), 1203–1209. <https://doi.org/10.5194/angeo-33-1203-2015>
- Bonfond, B., Yao, Z., & Grodent, D. (2020). Six pieces of evidence against the corotation enforcement theory to explain the main aurora at Jupiter. *Journal of Geophysical Research: Space Physics*, 125(11), e28152. <https://doi.org/10.1029/2020JA028152>
- Bougher, S. W., Waite, J. H., Majeed, T., & Gladstone, G. R. (2005). Jupiter Thermospheric General Circulation Model (JTGCM): Global structure and dynamics driven by auroral and Joule heating. *Journal of Geophysical Research: Planets*, 110(E4), E04008. <https://doi.org/10.1029/2003JE002230>
- Bunce, E. J., Arridge, C. S., Clarke, J. T., Coates, A. J., Cowley, S. W. H., Dougherty, M. K., et al. (2008). Origin of Saturn's aurora: Simultaneous observations by Cassini and the Hubble Space Telescope. *Journal of Geophysical Research: Space Physics*, 113(A9), A09209. <https://doi.org/10.1029/2008JA013257>
- Burleigh, M., Welling, D., Mukhopadhyay, A., & Liemohn, M. (2022). Impacts of 2-way coupling between the ionosphere and magnetosphere during the 2015 St. Patrick's Day storm. In *The Third Triennial Earth-Sun Summit (TESS)* (Vol. 54, p. 2022n7i125p40).
- Cavalié, T., Benmahi, B., Hue, V., Moreno, R., Lellouch, E., Fouchet, T., et al. (2021). First direct measurement of auroral and equatorial jets in the stratosphere of Jupiter. *Astronomy and Astrophysics*, 647, L8. <https://doi.org/10.1051/0004-6361/202140330>

## Acknowledgments

This work was supported by a NASA Keck PI Data Award, administered by the NASA Exoplanet Science Institute. Data presented herein were obtained at the W. M. Keck Observatory from telescope time allocated to the National Aeronautics and Space Administration through the agency's scientific partnership with the California Institute of Technology and the University of California. The Observatory was made possible by the generous financial support of the W. M. Keck Foundation. The authors wish to recognize and acknowledge the very significant cultural role and reverence that the summit of Maunakea has always had within the indigenous Hawaiian community. We are most fortunate to have the opportunity to conduct observations from this mountain. A portion of this research was carried out at the Jet Propulsion Laboratory, California Institute of Technology, under a contract with the National Aeronautics and Space Administration. R.W. was supported by a University of Leicester Doctoral Scholarship. M.N.C., E.M.T., P.I.T. were supported by UK Science and Technology Facilities Council (STFC) Studentship Grants ST/N504117/1, ST/T506242/1, and ST/X508548/1, respectively. K.L.N. was supported by a Northumbria University Doctoral Scholarship. T.S.S. was supported by UK STFC Consolidated Grants ST/W00089X/1. H.M. was supported by the STFC James Webb Fellowship ST/W001527/1 at the University of Leicester. L.M. was supported by Grant 80NSSC20K1045 issued through the NASA Solar System Workings program. J.O.D. was supported by a Japan Aerospace Exploration Agency (JAXA) International Top Young Fellowship. The authors thank Stan Cowley and Chihiro Tao for very useful discussions.

- Chané, E., Saur, J., Keppens, R., & Poedts, S. (2017). How is the Jovian main auroral emission affected by the solar wind? *Journal of Geophysical Research: Space Physics*, *122*(2), 1960–1978. <https://doi.org/10.1002/2016JA023318>
- Chané, E., Saur, J., & Poedts, S. (2013). Modeling Jupiter's magnetosphere: Influence of the internal sources. *Journal of Geophysical Research: Space Physics*, *118*(5), 2157–2172. <https://doi.org/10.1002/jgra.50258>
- Chaufray, J. Y., Greathouse, T. K., Gladstone, G. R., Waite, J. H., Maillard, J. P., Majeed, T., et al. (2011). Spectro-imaging observations of Jupiter's 2  $\mu\text{m}$  auroral emission. II: Thermospheric winds. *Icarus*, *211*(2), 1233–1241. <https://doi.org/10.1016/j.icarus.2010.11.021>
- Chowdhury, M. N., Stallard, T. S., Baines, K. H., Provan, G., Melin, H., Hunt, G. J., et al. (2022). Saturn's weather-driven aurorae modulate oscillations in the magnetic field and radio emissions. *Geophysics Research Letters*, *49*(3), e96492. <https://doi.org/10.1029/2021GL096492>
- Clarke, J. T., Nichols, J., Gérard, J. C., Grodent, D., Hansen, K. C., Kurth, W., et al. (2009). Response of Jupiter's and Saturn's auroral activity to the solar wind. *Journal of Geophysical Research: Space Physics*, *114*(A5), A05210. <https://doi.org/10.1029/2008JA013694>
- Connerney, J. E. P., Timmins, S., Oliverson, R. J., Espley, J. R., Joergensen, J. L., Kotsiaros, S., et al. (2022). A new model of Jupiter's magnetic field at the completion of Juno's prime mission. *Journal of Geophysical Research: Planets*, *127*(2), e07055. <https://doi.org/10.1029/2021JE007055>
- Cowley, S. W. H., & Bunce, E. J. (2001). Origin of the main auroral oval in Jupiter's coupled magnetosphere-ionosphere system. *Planetary and Space Science*, *49*(10–11), 1067–1088. [https://doi.org/10.1016/S0032-0633\(00\)00167-7](https://doi.org/10.1016/S0032-0633(00)00167-7)
- Cowley, S. W. H., & Bunce, E. J. (2003). Modulation of Jovian middle magnetosphere currents and auroral precipitation by solar wind-induced compressions and expansions of the magnetosphere: Initial response and steady state. *Planetary and Space Science*, *51*(1), 31–56. [https://doi.org/10.1016/S0032-0633\(02\)00130-7](https://doi.org/10.1016/S0032-0633(02)00130-7)
- Cowley, S. W. H., Bunce, E. J., & Nichols, J. D. (2003). Origins of Jupiter's main oval auroral emissions. *Journal of Geophysical Research: Space Physics*, *108*(A4), 8002. <https://doi.org/10.1029/2002JA009329>
- Cowley, S. W. H., Nichols, J. D., & Andrews, D. J. (2007). Modulation of Jupiter's plasma flow, polar currents, and auroral precipitation by solar wind-induced compressions and expansions of the magnetosphere: A simple theoretical model. *Annales Geophysicae*, *25*(6), 1433–1463. <https://doi.org/10.5194/angeo-25-1433-2007>
- Dunn, W. R., Gray, R., Wibisono, A. D., Lamy, L., Louis, C., Badman, S. V., et al. (2020). Comparisons between Jupiter's X-ray, UV and radio emissions and in-situ solar wind measurements during 2007. *Journal of Geophysical Research: Space Physics*, *125*(6), e27222. <https://doi.org/10.1029/2019JA027222>
- Gérard, J. C., Mura, A., Bonfond, B., Gladstone, G. R., Adriani, A., Hue, V., et al. (2018). Concurrent ultraviolet and infrared observations of the north Jovian aurora during Juno's first perijove. *Icarus*, *312*, 145–156. <https://doi.org/10.1016/j.icarus.2018.04.020>
- Grodent, D., Bonfond, B., Gérard, J.-C., Radioti, A., Gustin, J., Clarke, J. T., et al. (2008). Auroral evidence of a localized magnetic anomaly in Jupiter's northern hemisphere. *Journal of Geophysical Research: Space Physics*, *113*(A9), A09201. <https://doi.org/10.1029/2008JA013185>
- Grodent, D., Clarke, J. T., Kim, J., Waite, J. H., & Cowley, S. W. H. (2003). Jupiter's main auroral oval observed with HST-STIS. *Journal of Geophysical Research: Space Physics*, *108*(A11), 1389. <https://doi.org/10.1029/2003JA009921>
- Grodent, D., Clarke, J. T., Waite, J. H., Cowley, S. W. H., Gérard, J. C., & Kim, J. (2003). Jupiter's polar auroral emissions. *Journal of Geophysical Research: Space Physics*, *108*(A10), 1366. <https://doi.org/10.1029/2003JA010017>
- Hill, T. W. (1979). Inertial limit on corotation. *Journal of Geophysical Research*, *84*(A11), 6554–6558. <https://doi.org/10.1029/JA084iA11p06554>
- Hill, T. W. (2001). The Jovian auroral oval. *Journal of Geophysical Research*, *106*(A5), 8101–8108. <https://doi.org/10.1029/2000JA000302>
- Hong, Y., Deng, Y., Zhu, Q., Maute, A., Hairston, M. R., Waters, C., et al. (2023). Inter-hemispheric asymmetries in high-latitude electrodynamic forcing and the thermosphere during the October 8–9, 2012, geomagnetic storm: An integrated data–model investigation. *Frontiers in Astronomy and Space Sciences*, *10*, 34. <https://doi.org/10.3389/fspas.2023.1062265>
- Huang, T. S., & Hill, T. W. (1989). Corotation lag of the Jovian atmosphere, ionosphere, and magnetosphere. *Journal of Geophysical Research*, *94*(A4), 3761–3765. <https://doi.org/10.1029/JA094iA04p03761>
- Johnson, R. E., Stallard, T. S., Melin, H., Nichols, J. D., & Cowley, S. W. H. (2017). Jupiter's polar ionospheric flows: High resolution mapping of spectral intensity and line-of-sight velocity of  $\text{H}^+$  ions. *Journal of Geophysical Research: Space Physics*, *122*(7), 7599–7618. <https://doi.org/10.1002/2017JA024176>
- Kane, M., Mitchell, D. G., Carbary, J. F., Dialynas, K., Hill, M. E., & Krimigis, S. M. (2020). Convection in the magnetosphere of Saturn during the Cassini mission derived from MIMI INCA and CHEMS measurements. *Journal of Geophysical Research: Space Physics*, *125*(2), e27534. <https://doi.org/10.1029/2019JA027534>
- Khurana, K. K. (2001). Influence of solar wind on Jupiter's magnetosphere deduced from currents in the equatorial plane. *Journal of Geophysical Research*, *106*(A11), 25999–26016. <https://doi.org/10.1029/2000JA000352>
- Khurana, K. K., Dougherty, M. K., Provan, G., Hunt, G. J., Kivelson, M. G., Cowley, S. W. H., et al. (2018). Discovery of atmospheric-wind-driven electric currents in Saturn's magnetosphere in the gap between Saturn and its rings. *Geophysics Research Letters*, *45*(19), 10068–10074. <https://doi.org/10.1029/2018GL078256>
- Kita, H., Fujisawa, S., Tao, C., Kagitani, M., Sakanoi, T., & Kasaba, Y. (2018). Horizontal and vertical structures of Jovian infrared aurora: Observation using Subaru IRCS with adaptive optics. *Icarus*, *313*, 93–106. <https://doi.org/10.1016/j.icarus.2018.05.002>
- Kivelson, M. G., & Southwood, D. J. (2005). Dynamical consequences of two modes of centrifugal instability in Jupiter's outer magnetosphere. *Journal of Geophysical Research: Space Physics*, *110*(A12), A12209. <https://doi.org/10.1029/2005JA011176>
- Kotsiaros, S., Connerney, J. E. P., Clark, G., Allegrini, F., Gladstone, G. R., Kurth, W. S., et al. (2019). Birkeland currents in Jupiter's magnetosphere observed by the polar-orbiting Juno spacecraft. *Nature Astronomy*, *3*(10), 904–909. <https://doi.org/10.1038/s41550-019-0819-7>
- Krupp, N., Lagg, A., Livi, S., Wilken, B., Woch, J., Roelof, E. C., & Williams, D. J. (2001). Global flows of energetic ions in Jupiter's equatorial plane: First-order approximation. *Journal of Geophysical Research*, *106*(A11), 26017–26032. <https://doi.org/10.1029/2000JA900138>
- Mauk, B. H., Clark, G., Gladstone, G. R., Kotsiaros, S., Adriani, A., Allegrini, F., et al. (2020). Energetic particles and acceleration regions over Jupiter's polar cap and main aurora: A broad overview. *Journal of Geophysical Research: Space Physics*, *125*(3), e27699. <https://doi.org/10.1029/2019JA027699>
- McLean, I. S., Becklin, E. E., Bendiksen, O., Brims, G., Canfield, J., Figer, D. F., et al. (1998). Design and development of NIRSPEC: A near-infrared echelle spectrograph for the Keck II telescope. In A. M. Fowler (Ed.), *Infrared astronomical instrumentation* (Vol. 3354, pp. 566–578). <https://doi.org/10.1117/12.317283>
- Millward, G., Miller, S., Stallard, T., Achilleos, N., & Aylward, A. D. (2005). On the dynamics of the jovian ionosphere and thermosphere. IV. Ion-neutral coupling. *Icarus*, *173*(1), 200–211. <https://doi.org/10.1016/j.icarus.2004.07.027>
- Nichols, J. D., Badman, S. V., Bunce, E. J., Clarke, J. T., Cowley, S. W. H., Crary, F. J., et al. (2009). Saturn's equinoctial auroras. *Geophysics Research Letters*, *36*(24), L24102. <https://doi.org/10.1029/2009GL041491>
- Nichols, J. D., Bunce, E. J., Clarke, J. T., Cowley, S. W. H., Gérard, J. C., Grodent, D., & Pryor, W. R. (2007). Response of Jupiter's UV auroras to interplanetary conditions as observed by the Hubble Space Telescope during the Cassini flyby campaign. *Journal of Geophysical Research: Space Physics*, *112*(A2), A02203. <https://doi.org/10.1029/2006JA012005>

- Nichols, J. D., Clarke, J. T., Gérard, J. C., Grodent, D., & Hansen, K. C. (2009). Variation of different components of Jupiter's auroral emission. *Journal of Geophysical Research: Space Physics*, 114(A6), A06210. <https://doi.org/10.1029/2009JA014051>
- Nichols, J. D., & Cowley, S. W. H. (2022). Relation of Jupiter's dawnside main emission intensity to magnetospheric currents during the Juno mission. *Journal of Geophysical Research: Space Physics*, 127(1), e30040. <https://doi.org/10.1029/2021JA030040>
- Porco, C. C., West, R. A., McEwen, A., DelGenio, A. D., Ingersoll, A. P., Thomas, P., et al. (2003). Cassini imaging of Jupiter's atmosphere, satellites, and rings. *Science*, 299(5612), 1541–1547. <https://doi.org/10.1126/science.1079462>
- Ray, L. C., Achilleos, N. A., Vogt, M. F., & Yates, J. N. (2014). Local time variations in Jupiter's magnetosphere-ionosphere coupling system. *Journal of Geophysical Research: Space Physics*, 119(6), 4740–4751. <https://doi.org/10.1002/2014JA019941>
- Sangalli, L., Knudsen, D. J., Larsen, M. F., Zhan, T., Pfaff, R. F., & Rowland, D. (2009). Rocket-based measurements of ion velocity, neutral wind, and electric field in the collisional transition region of the auroral ionosphere. *Journal of Geophysical Research: Space Physics*, 114(A4), A04306. <https://doi.org/10.1029/2008JA013757>
- Smith, C. G. A. (2013). Electrodynamic coupling of Jupiter's thermosphere and stratosphere: A new source of thermospheric heating? *Icarus*, 226(1), 923–944. <https://doi.org/10.1016/j.icarus.2013.07.001>
- Smith, C. G. A., & Aylward, A. D. (2009). Coupled rotational dynamics of Jupiter's thermosphere and magnetosphere. *Annales Geophysicae*, 27(1), 199–230. <https://doi.org/10.5194/angeo-27-199-2009>
- Southwood, D. J., & Kivelson, M. G. (2001). A new perspective concerning the influence of the solar wind on the Jovian magnetosphere. *Journal of Geophysical Research*, 106(A4), 6123–6130. <https://doi.org/10.1029/2000JA000236>
- Stallard, T. S., Clarke, J. T., Melin, H., Miller, S., Nichols, J. D., O'Donoghue, J., et al. (2016). Stability within Jupiter's polar auroral 'Swirl region' over moderate timescales. *Icarus*, 268, 145–155. <https://doi.org/10.1016/j.icarus.2015.12.044>
- Stallard, T. S., Miller, S., Cowley, S. W. H., & Bunce, E. J. (2003). Jupiter's polar ionospheric flows: Measured intensity and velocity variations poleward of the main auroral oval. *Geophysics Research Letters*, 30(5), 1221. <https://doi.org/10.1029/2002GL016031>
- Stallard, T. S., Miller, S., Millward, G., & Joseph, R. D. (2001). On the dynamics of the jovian ionosphere and thermosphere. I. The measurement of ion winds. *Icarus*, 154(2), 475–491. <https://doi.org/10.1006/icar.2001.6681>
- Stallard, T. S., Miller, S., Trafton, L. M., Geballe, T. R., & Joseph, R. D. (2004). Ion winds in Saturn's southern auroral/polar region. *Icarus*, 167(1), 204–211. <https://doi.org/10.1016/j.icarus.2003.09.006>
- Tao, C., Badman, S. V., & Fujimoto, M. (2011). UV and IR auroral emission model for the outer planets: Jupiter and Saturn comparison. *Icarus*, 213(2), 581–592. <https://doi.org/10.1016/j.icarus.2011.04.001>
- Tao, C., Fujiwara, H., & Kasaba, Y. (2009). Neutral wind control of the Jovian magnetosphere-ionosphere current system. *Journal of Geophysical Research: Space Physics*, 114(A8), A08307. <https://doi.org/10.1029/2008JA013966>
- Thayer, J. P. (2000). High-latitude currents and their energy exchange with the ionosphere-thermosphere system. *Journal of Geophysical Research*, 105(A10), 23015–23024. <https://doi.org/10.1029/1999JA000409>
- Uno, T., Kasaba, Y., Tao, C., Sakanoi, T., Kagitani, M., Fujisawa, S., et al. (2014). Vertical emissivity profiles of Jupiter's northern H<sub>3</sub><sup>+</sup> and H<sub>2</sub> infrared auroras observed by Subaru/IRCS. *Journal of Geophysical Research: Space Physics*, 119(12), 10219–10241. <https://doi.org/10.1002/2014JA020454>
- Walterscheid, R. L., & Crowley, G. (2015). Thermal cell structures in the high-latitude thermosphere induced by ion drag. *Journal of Geophysical Research: Space Physics*, 120(8), 6837–6850. <https://doi.org/10.1002/2015JA021122>
- Yao, Z. H., Bonfond, B., Grodent, D., Chané, E., Dunn, W. R., Kurth, W. S., et al. (2022). On the relation between auroral morphologies and compression conditions of Jupiter's magnetopause: Observations from Juno and the Hubble Space Telescope. *Journal of Geophysical Research: Space Physics*, 127(10), e2021JA029894. <https://doi.org/10.1029/2021JA029894>
- Yates, J. N., Ray, L. C., Achilleos, N., Witasse, O., & Altobelli, N. (2020). Magnetosphere-ionosphere-thermosphere coupling at Jupiter using a three-dimensional atmospheric general circulation model. *Journal of Geophysical Research: Space Physics*, 125(1), e26792. <https://doi.org/10.1029/2019JA026792>

## References From the Supporting Information

- Kim, S., Prato, L., & McLean, I. (2015). REDSPEC: NIRSPEC data reduction.
- Lindsay, C. M., & McCall, B. J. (2001). Comprehensive evaluation and compilation of H<sub>3</sub><sup>+</sup> spectroscopy. *Journal of Molecular Spectroscopy*, 210(1), 60–83. <https://doi.org/10.1006/jmsp.2001.8444>
- Lord, S. D. (1992). *A new software tool for computing Earth's atmospheric transmission of near- and far-infrared radiation* (p. 103957). NASA Technical Memorandum.
- Moses, J. I., & Bass, S. F. (2000). The effects of external material on the chemistry and structure of Saturn's ionosphere. *Journal of Geophysical Research*, 105(E3), 7013–7052. <https://doi.org/10.1029/1999JE001172>
- Neale, L., Miller, S., & Tennyson, J. (1996). Spectroscopic properties of the H<sub>3</sub><sup>+</sup> molecule: A new calculated line list. *The Astrophysical Journal*, 464, 516. <https://doi.org/10.1086/177341>
- Newville, M., Stensitzki, T., Allen, D. B., Rawlik, M., Ingargiola, A., & Nelson, A. (2016). Lmfit: Non-linear least-square minimization and curve-fitting for python.
- Stallard, T. S., Baines, K. H., Melin, H., Bradley, T. J., Moore, L., O'Donoghue, J., et al. (2019). Local-time averaged maps of H<sub>3</sub><sup>+</sup> emission, temperature and ion winds. *Philosophical Transactions of the Royal Society of London, Series A*, 377(2154), 20180405. <https://doi.org/10.1098/rsta.2018.0405>